1 Organic aerosol source apportionment by offline-AMS over a full

2 year in Marseille

4 **Carlo Bozzetti[1], Imad El Haddad[1], Dalia Salameh[2,7], Kaspar Rudolf Daellenbach[1], Paola**

5 **Fermo[3], Raquel Gonzalez[3], Maria Cruz Minguillón[4], Yoshiteru Iinuma[5], Laurent**

6 **Poulain[5], Emanuel Müller[6], Jay Gates Slowik[1], Jean-Luc Jaffrezo[7], Urs Baltensperger[1],**

7 **Nicolas Marchand[2], and André Stephan Henry Prévôt[1]**

8 [1]{Paul Scherrer Institute (PSI), 5232 Villigen-PSI, Switzerland }

9 [2]{Aix Marseille Univ., CNRS, LCE, 13331 Marseille, France}

10 [3]{Università degli Studi di Milano, 20133 Milano, Italy}

11 [4]{Institute of Environmental Assessment and Water Research (IDAEA), CSIC, 08034

12 Barcelona, Spain}

13 [5]{Leibniz Institute für Troposphärenforschung, 04318 Leipzig, Germany}

14 [6]{Eawag, 8600 Dübendorf, Switzerland}

15 [7]{Université Grenoble Alpes, CNRS, LGGE, 38000 Grenoble, France}

17 Correspondence to: A. S. H. Prévôt (andre.prevot@psi.ch)

18   N. Marchand (nicolas.marchand@univ-amu.fr)

20 Abstract

21 We investigated the seasonal trends of OA sources affecting the air quality of Marseille

22 (France) which is the largest harbor of the Mediterranean Sea. This was achieved by

23 measurements of nebulized filter extracts using an aerosol mass spectrometer (offline-AMS).

24 $PM_{2.5}$ (particulate matter with an aerodynamic diameter <2.5 µm) filter samples were

25 collected over 1 year from August 2011 to July 2012. The same samples were also analyzed

26 for major water-soluble ions, metals, elemental and organic carbon (EC/OC), and organic

27 markers, including n-alkanes, hopanes, polyaromatic hydrocarbons (PAHs), lignin and

28 cellulose pyrolysis products and nitrocatechols. The application of positive matrix

factorization (PMF) to the water-soluble AMS spectra enabled the extraction of five factors, related to hydrocarbon-like OA (HOA), cooking OA (COA), biomass burning OA (BBOA), oxygenated OA (OOA), and an industry-related OA (INDOA). Seasonal trends and relative contributions of OA sources were compared with the source apportionment of OA spectra collected from the AMS field deployment at the same station but in different years and for shorter monitoring periods (February 2011 and July 2008). Online- and offline-AMS source apportionment revealed comparable seasonal contribution of the different OA sources. Results revealed that BBOA was the dominant source during winter representing on average 48% of the OA, while during summer the main OA component was OOA (63% of OA mass on average). HOA related to traffic emissions contributed on a yearly average 17% to the OA mass, while COA was a minor source contributing 4%. The contribution of INDOA was enhanced during winter (17% during winter and 11% during summer), consistent with an increased contribution from light alkanes, light PAHs (fluoranthene, pyrene, phenanthrene) and selenium, which is commonly considered as an unique coal combustion and coke production marker. Online- and offline-AMS source apportionments revealed evolving levoglucosan:BBOA ratios, being higher during late autumn and March. A similar seasonality was observed in the ratios of cellulose combustion markers to lignin combustion markers, highlighting the contribution from cellulose rich biomass combustion, possibly related to agricultural activities.

1 Introduction

Outdoor particulate air pollution is estimated to be responsible for approximately 3.3 million premature deaths each year worldwide, and this number is projected to double by 2050 (Lelieveld et al., 2015). Organic aerosols (OA) can contribute up to 90% of the PM_1 (Jimenez et al., 2009), therefore understanding their main emission sources and formation processes is a key prerequisite for the development of appropriate mitigation policies.

In the Mediterranean basin, sources and trends of OA remain scarcely investigated, despite their deleterious impact in such a densely populated region. The Mediterranean region is characterized by an intense photochemistry during summer. Not surprisingly, the majority of the OA source apportionment studies conducted in the region using aerosol mass spectrometry (AMS) focused on the summer period (e.g., El Haddad et al., 2013; Minguillón et al., 2011, 2016; Hildebrandt et al., 2011). Through positive matrix factorization (PMF)

1   techniques, these studies revealed that during summer the oxygenated organic aerosol (OOA)

2   fraction formed by oxidation of gaseous precursors, represented the largest part of OA.

3   Amongst these studies, the field deployment of the AMS in Marseille, the largest port in the

4   Mediterranean, has demonstrated that this instrument is well suited for quantifying the

5   contribution of industrial emissions (El Haddad et al., 2013). In that work, the industrial OA

6   factor was identified by the high correlation with heavy metals and AMS-polycyclic aromatic

7   hydrocarbons (AMS-PAHs), moreover strong increments of the industrial factor

8   concentrations were systematically observed when winds shifted to the west/south west,

9   consistent with back-trajectory analysis highlighting the transport of industrial emissions from

10   an industrial pole. Overall the industry-related OA contributed on average 7% of the bulk OA

11   mass (El Haddad et al., 2011; 2013). However, these results were limited to 2 weeks of

12   measurements during summer while the contribution of industrial emissions during the rest of

13   the year remains unknown.

14   There is a general paucity of AMS and ACSM datasets in the Mediterranean region during

15   winter. Exceptions include AMS campaigns (Mohr et al. 2012; Hildebrandt et al., 2011)

16   covering a few weeks during late winter-early spring, and studies with an aerosol chemical

17   speciation monitor (ACSM) (e.g., Minguillón et al., 2015, covering three weeks of

18   monitoring). The measurement of organic markers and elements (e.g., Salameh et al., 2015;

19   Reche et al., 2012) at different stations indicate a substantial contribution from biomass

20   burning (BB). However, the sources and chemical composition of this fraction and its

21   evolution during the year remain uncertain. Modelling results within the European Monitoring

22   and Evaluation Programme (EMEP) have shown that the South of France, together with

23   Portugal, can be a major hot spot in Europe for OA during February-March, possibly due to

24   agricultural fires (Dernier van der Gon et al., 2015; Fountoukis et al., 2014). In this region,

25   BBOA can derive from various processes such as agricultural land clearing activities,

26   wildfires, and domestic heating, and therefore may have a variable chemical composition.

27   The current study capitalizes on the AMS measurements of offline samples collected over one

28   year (2011-2012), in Marseille, an ideal environment for the characterization of urban

29   emissions from biomass burning, traffic and industrial activities and their transformation

30   under high photochemical activity. The source apportionment results obtained from PMF

31   applied to the OA mass spectra are corroborated using a comprehensive set of offline

32   measurements including elemental and organic carbon (EC/OC) measurements, as well as

1 measurements of elements by inductively coupled plasma mass spectrometry (ICP-MS), of

2 molecular markers by gas chromatography mass spectrometry (GC-MS) and ultra-

3 performance liquid chromatography mass spectrometry (UPLC-MS), and of major ions by ion

4 chromatography (IC). We mainly focus on the sources and trends of winter OA and therefore

5 we additionally analyzed an online AMS dataset acquired at the same location during the

6 winter of the previous year. The comparison of online- and offline-AMS data, and organic

7 marker concentrations enables an in-depth characterization of OA sources in Marseille, and in

8 particular the identification of the main processes by which biomass smoke is emitted and

9 transformed in this region.

2   Methods

2.1 Site description

13 Marseille is the second largest city in France with more than 1 million inhabitants (2010). It

14 hosts the largest harbor in France and in the Mediterranean Sea. Many port-related industries,

15 especially petrochemical companies, are located in a big cluster. These facilities are situated

16 about 40 km NW from the city and include steel facilities, coke production plants, oil storing,

17 refining plants, and several shipyards. The Marseille commercial harbor is located in the

18 vicinity of this industrial cluster and represents the third-largest harbor of the world for crude

19 oil storage and treatment. During summer, typical wind patterns in the city of Marseille favor

20 the transport of polluted air masses from the industrial cluster to the city, including the sea

21 breeze and the light Mistral wind from the Rhone valley. At night, the land breeze may

22 transport air masses from an agricultural valley located east of the sampling site. A more

23 detailed description of wind patterns in Marseille can be found in Drobinski et al. (2007) and

24 Flaounas et al. (2009). The sampling location is classified as an urban background station and

25 is situated in the urban park "Cinq Avenue" in a traffic-free zone near the city center

26 (43°18'20'' N, 5°23'40''E; 64 m a.s.l.).

1 **2.2 Yearly cycle dataset**

2 *Sample collection.*

3 In total, 216 24-h (from midnight-to-midnight) integrated $PM_{2.5}$ pre-baked (500°C for 3 h)

4 quartz fiber filters (150 mm diameter, Tissuquartz) were collected between 30 July 2011 and

5 20 July 2012 using a High-Volume sampler (Digitel DA80) operated at 500 L min^{-1} (Batch 1).

6 Filter samples were subsequently wrapped in aluminum foil, sealed in polyethylene bags and

7 stored at -18°C.

8 *Offline-AMS analysis.* This work discusses the offline-AMS analysis of 55 composite samples

9 (created from the batch of 216 $PM_{2.5}$ filters collected) which were analyzed by Salameh et al.

10 (*in prep.*) for major ions, molecular markers and elements (Table S1). A thorough description

11 of the offline-AMS analysis can be found in Daellenbach et al. (2016). One punch per filter

12 sample (from 5 to 25 mm diameter depending on the filter loading and on the number of

13 punches per composite sample) was prepared for analysis. Punches from the same composite

14 sample were extracted together in 15 mL of ultrapure water (18.2 MΩ cm, total organic

15 carbon < 5ppb, 25°C) in an ultrasonic bath for 20 min at 30°C. After extraction, filters were

16 vortexed for 1 min, and the resulting liquids were filtered with 0.45 μm nylon membrane

17 syringe filters.

18 The generated liquid extracts were atomized in air using a custom-made two-nozzle nebulizer.

19 The generated aerosol was dried using a silica gel diffusion drier and then measured by a high

20 resolution time-of-flight AMS (HR-ToF-AMS, running in V-mode). In the AMS, particles are

21 flash vaporized (600°C) and the resulting gas is then ionized by electron impact (EI, 70eV),

22 yielding quantitative mass spectra of the non-refractory submicron aerosol components,

23 including OA, NO_3^-, SO_4^{2-}, NH_4^+, and Cl^-. A detailed description of the AMS operating

24 principles, calibration protocols, and analysis procedures are provided by DeCarlo et al.

25 (2006). In total about 10 mass spectra (mass range 12-300 Da, 60 sec averaging time) were

26 collected per composite sample. Between each sample, a measurement blank was recorded via

27 nebulization of ultra-pure water to minimize and monitor the possible memory effects of the

28 system. In total five mass spectra were collected per each measurement blank. Offline-AMS

29 data were processed and analyzed using the HR-ToF-AMS analysis software SQUIRREL

30 (SeQUential Igor data RetRiEvaL) v.1.52L and PIKA (Peak Integration by Key Analysis)

31 v.1.11L for IGOR Pro software package (Wavemetrics, Inc., Portland, OR, USA). HR

1 analysis of the mass spectra was performed in the mass range 12-115 Da and in total 217 ion

2 fragments were fitted.

3 The interference of NH_4NO_3 on the CO_2^+ signal was corrected according to Pieber et al.

4 (2016) as follows:

5 $$CO_{2,real} = CO_{2,meas} - \left(\frac{CO_{2,meas}}{NO_{3,meas}}\right)_{NH_4NO_3,pure} * NO_{3,meas}$$

6   (1)

7 where the $\left(\frac{CO_{2,meas}}{NO_{3,meas}}\right)_{NH_4NO_3,pure}$ correction factor was 2.5% as determined from aqueous

8 NH_4NO_3 measurements conducted regularly during the measurement period.

9 *Other offline measurements.* A complete list of the measurements performed can be found in

10 Table S1. To summarize, major ions (Ca^{2+}, Mg^{2+}, K^+, Na^+, NH_4^+, NO_3^-, SO_4^{2-}, Cl^-, oxalate,

11 malate, succinate, and malonate) were measured by ion chromatography (IC) according to the

12 methodology described by Jaffrezo et al. (1998). A subset of the filters was selected for CO_3^{2-}

13 quantification following the method described by Karanasiou et al. (2011). The method

14 encompasses the fumigation of the filter samples with HCl. The CO_2 evolved by this

15 acidification of the carbonates deposited on the filters is detected by thermal optical

16 transmittance determination. The CO_3^{2-} measurements agreed fairly well with the CO_3^{2-}

17 estimate from ion balance calculations based on IC data (Fig. S1). In the following discussion,

18 ion concentrations from filter samples always refer to the IC measurements unless otherwise

19 specified.

20 Elemental and organic carbon (EC and OC) were determined for each filter by thermal optical

21 transmittance using a Sunset Lab analyzer (Birch and Cary, 1996) following the EUSAAR2

22 protocol (Cavalli et al., 2010). The CO_3^{2-} concentration determined from the IC ion balance

23 was then subtracted from OC concentration. The water soluble OC (WSOC) was measured

24 with a total organic carbon analyzer (TOC) following the methodology described in Bozzetti

25 et al. (2016a) and references therein. Before the analyses, the liquid extracts were treated with

26 a 2 M HCl solution for 1-30 min to remove the inorganic C fraction. Total nitrogen (TN) was

27 determined using a TOC analyzer combustion tube. The NO_2 generated from the water

28 soluble (WS) N decomposition was detected by a chemiluminescence TNM-1 unit detector.

29 Organic markers were measured via GC-MS analysis, following the methodology described

30 in El Haddad et al. (2009; 2011), Favez et al. (2010) and Piot et al. (2012). In total 15

31 different polycyclic aromatic hydrocarbons (PAH), 19 alkanes (C19-C36), 8 hopanes, 5

1   phtalate esters, levoglucosan, 6 lignin pyrolysis compounds, 6 fatty acids, and 3 sterols were

2   determined (Table S1). 33 chemical elements (Table S1) were quantified using ICP-MS

3   according to the procedure described in Chauvel et al. (2010) and the modifications suggested

4   in El Haddad et al. (2011). A subset of 20 composite samples was selected for the

5   quantification of methyl-nitrocatechol isomers (Table S1) via Ultra Performance Liquid

6   Chromatography coupled with an Electro Spray Ionization – ToF - MS (UPLC-ESI-ToF-MS),

7   following the procedure described in Iinuma et al. (2010).

8   **2.3 Intensive winter campaign**

9   A HR-ToF-AMS was deployed at the same station (urban park "Cinq Avenue") between 25

10 January 2011 and 2 March 2011 to monitor the real-time NR-PM$_1$ aerosol chemical

11 composition. Although February 2011 is not included in the sampling period covered by

12 offline-AMS, these online measurements nonetheless provide a good opportunity to compare

13 the separation, relative contributions and winter seasonal trends of the OA sources retrieved

14 by the offline- and online-AMS source apportionment procedures. Summer offline-AMS

15 results were instead compared with online-AMS source apportionment results reported by El

16 Haddad et al. (2013). The AMS was operated with an averaging time of 8 minutes, and in

17 total 5633 mass spectra were collected during the monitoring period. We performed an

18 ionization efficiency (IE) calibration by NH$_4$NO$_3$ nebulization, and the resulting IE value of

19 $1.76 \cdot 10^{-7}$ was applied to the dataset. The standard relative ionization (RIE) efficiency was

20 assumed for organics (1.4), SO$_4^{2-}$ (1.2), NH$_4^+$ (4) and Cl$^-$ (1.3), while the collection efficiency

21 (CE) was estimated using the composition dependent collection efficiency model

22 (Middlebrook et al., 2012). Total AMS-PAHs were estimated from AMS data according to

23 Dzepina et al. (2007).

24 Similarly to offline-AMS, online-AMS data were also processed and analyzed using HR-ToF-

25 AMS Analysis software SQUIRREL (SeQUential Igor data RetRiEvaL) v.1.52L and PIKA

26 (Peak Integration by Key Analysis) v.1.11L for IGOR Pro software package (Wavemetrics,

27 Inc., Portland, OR, USA). HR analysis of the mass spectra was performed in the mass range

28 12-115 Da and in total 215 ion fragments were fitted.

29 A NO$_x$ analyzer was run in parallel to the AMS to monitor the real-time NO$_x$ concentration. A

30 set of pre-baked (500°C for 3h) 24-h integrated PM$_{2.5}$ filter samples was also collected during

31 this campaign (Batch 2) following the same sampling and storage procedure described in

1 Section 2.2. Filters were analyzed for major ions, metals, elemental and organic carbon

2 (EC/OC), and organic markers, including n-alkanes, hopanes, polyaromatic hydrocarbons

3 (PAHs), lignin and cellulose pyrolysis products using the techniques previously described in

4 Section 2.2 (Table S1).

6 **2.4 Source apportionment**

7 *Implementation.* The online- and offline-AMS source apportionment results discussed in this

8 work were obtained from PMF analysis (Paatero and Tapper, 1994) of AMS spectra using the

9 Multilinear Engine (ME-2, Paatero 1999). The Source Finder toolkit (SoFi, Canonaco et al.,

10 2013, v.5.1) for Igor Pro (Wavemetrics, Inc., Portland, OR, USA) served as interface for data

11 input and results evaluation. PMF is a multilinear statistical tool used to describe the

12 variability of a multivariate dataset as the linear combination of static factor profiles times

13 their corresponding time series, as described in Eq. 2:

14 $$x_{i,j} = \sum_{z=1}^{p} g_{i,z} \cdot f_{z,j} + e_{i,j} \qquad (2)$$

15 Here $x_{i,j}$, $g_{i,z}$, $f_{z,j}$, and $e_{i,j}$ represent respectively elements of the data matrix, factor time series

16 matrix, factor profile matrix and residual matrix, while subscripts i,j and z denote time

17 elements, variables (in our case AMS fragments), and discrete factor numbers, respectively. p

18 represents the total number of factors selected by the user for current given PMF solution. The

19 PMF algorithm returns only $g_{i,z}$ and $f_{z,j}$ values ≥ 0, and solves Eq. 2 by minimizing the object

20 function Q, defined as:

21 $$Q = \sum_i \sum_j \left(\frac{e_{i,j}}{s_{i,j}}\right)^2 \qquad (3)$$

22 Here $s_{i,j}$ is an element of the error input matrix. PMF is subject to rotational ambiguity, i.e.

23 different $\mathbf{G} \cdot \mathbf{F}$ combinations characterized by the same Q can exist. The ME-2 implementation

24 of the PMF algorithm offers an efficient exploration of the solution space by directing the

25 solution toward environmentally-meaningful rotations by constraining the factor profile

26 elements $f_{z,j}$ for one or more z factors. In the *a*-value implementation of ME-2, the elements of

27 the factor profile matrix $\mathbf{F}$ (in our case AMS fragments) are forced to predefined values $f_{z,j}$

28 allowing a certain variability defined by the *a*-value, such that the modelled element $f_{z,j}'$

29 satisfies Eq. 4:

1 $$\frac{(1-a)f_{z,n}}{(1+a)f_{z,m}} \le \frac{f_{z,n'}}{f_{z,m'}} \le \frac{(1+a)f_{z,n}}{(1-a)f_{z,m}}$$ (4)

2   where n and m represent any two arbitrary variables in the normalized **F** matrix. A complete

3   description of the a-value approach can be found elsewhere (Canonaco et al., 2013).

4   For the offline–AMS source apportionment, the PMF input data matrix was constructed as

5   follows: each composite sample is represented by approximately 10 time points i,

6   corresponding to the ~10 mass spectra collected per filter sample (section 2.4). Each point of

7   the data matrix is subtracted by the average corresponding measurement blank.

8   The error matrices were instead constructed as follows. For online-AMS source

9   apportionment, the error matrix elements $s_{i,j}$ were calculated according to Allan et al. (2003)

10 and Ulbrich et al. (2009), and included the uncertainty deriving from electronic noise, ion-to-

11 ion variability at the detector, and ion counting statistics. $s_{i,j}$ included also a minimum error

12 which was applied according to Ulbrich et al. (2009). For the offline-AMS source

13 apportionment, the error term $\delta_{i,j}$ was calculated in the same way, but a further term ($\sigma_{i,j}$)

14 including the blank subtraction uncertainty was propagated according to Eq. 5:

15 $$s_{i,j} = \sqrt{\delta_{i,j}^2 + \sigma_{i,j}^2}$$ (5)

16 Finally for both online- and offline-AMS we applied a down-weighting factor of 3 to all

17 variables with an average signal to an average error ratio lower than 2 (Ulbrich et al., 2009).

18 No variable with an average signal to error value lower than 0.2 was detected.

19 Dust and ash can contain significant amount of inorganic CO_3^{2-}. Both the IC balance and the

20 CO_3^{2-} measurements revealed non-negligible contributions from CO_3^{2-} in the $PM_{2.5}$ fraction

21 (Fig. S1). Preliminary PMF results also resolved a factor correlating with Ca^{2+} (SI) which was

22 characterized by high $f CO_2^+$, suggesting a possible solubilisation of CO_3^{2-} from dust which

23 could affect the OA mass spectral fingerprint. Overall, as discussed in the SI, we could not

24 achieve a clear inorganic dust separation using PMF, therefore we opted for a correction of

25 the PMF input matrices. The measured pH of our filter extracts was never >8, therefore we

26 can exclude the presence of CO_3^{2-} in the extracts, but rather assume all solubilized CO_3^{2-} to

27 exist as HCO_3^-. Direct measurements of nebulized standard $NaHCO_3$ aqueous solutions,

28 revealed that thermal decomposition of HCO_3^- on the AMS vaporizer (600°C) releases CO_2

29 (Fig. S2). Currently no HCO_3^- correction for the OA spectra is implemented in the standard

30 AMS fragmentation table (Aiken et al., 2008), therefore the measured CO_2^+ signal needs to be

1   subtracted from the OA AMS spectra. Offline-AMS PMF input matrices were corrected for

2   HCO_3^- and rescaled for $WSOM_i$ according to the procedure described in the Supplementary

3   information, SI.

4   *Online-AMS source apportionment optimization*. In the following we describe the

5   optimization of the online-AMS source apportionment results. In order to optimize the source

6   separation we performed sensitivity analyses on PMF solutions. We adopted different

7   optimization strategies for online- and offline-AMS source apportionments (SI) as we

8   encountered dissimilar mixings between sources. This is not surprising as the two methods are

9   characterized by different time resolution and different monitoring time extension (1 year for

10   offline-AMS, 1 month for online-AMS), which in turn result in different variabilities

11   apportioned by the PMF algorithm (daily for online-AMS *vs.* seasonal for offline-AMS).

12   We selected a 4-factor solution based on residual analysis. We investigated the time

13   dependent $Q(t)/Q_{exp}(t)$ evolution when increasing the number of factors. Q/Q_{exp} is defined as

14   the ratio between Q (as defined in Eq. 3) and the remaining degrees of freedom of the model

15   solution (Q_{exp}) calculated as $i·j-(j+i)p$ (Canonaco et al., 2013). A decrease of the Q/Q_{exp}, from

16   lower to higher order solutions indicates an improvement in the variation explained by the

17   model. In particular we calculated the $\Delta(Q/Q_{exp}(t))$ obtained as the difference between the

18   $Q/Q_{exp}(t)$ for a (z)–factor solution minus the $Q/Q_{exp}(t)$ value obtained from the (z-1)–factor

19   solutions, where z indicates the number of factors. We observed a large reduction of

20   $\Delta(Q/Q_{exp}(t))$ until 4 factors (Fig. S4). Higher order solutions provided only minor

21   contributions to the explained variability and in terms of solution interpretability resulted in a

22   splitting of primary sources which could not be unambiguously associated to specific aerosol

23   sources or processes. An *a*-value sensitivity analysis was performed by scanning all possible

24   *a*-value combinations for HOA and COA given by an *a*-value range 0-1 with a step size of

25   0.1. In order to optimize the source apportionment results, we retained only the PMF solutions

26   satisfying an acceptance criterion described hereafter.

27   PMF factors were associated to specific aerosol emissions/processes based on mass spectral

28   features, diurnal cycles, and time series correlations with tracers. The identified factors were

29   associated to traffic (HOA), cooking (COA), biomass burning (BBOA), and oxygenated

30   organic aerosol (OOA). A thorough interpretation of the PMF factors will be discussed in the

31   Results section. Given the absence of widely accepted tracers for COA emissions, the

32   optimization of the COA contributions was based on the analysis of the COA diurnal cycles.

33   PMF solutions obtained from the COA and HOA *a*-value sensitivity analysis (121 PMF runs

1   in total) were categorized according to a cluster analysis of the normalized COA diurnal

2   cycles (Elser et al. 2015 and references therein). The k-means clustering approach enables

3   classifying the PMF solutions into k clusters, by minimizing a cost function (C):

4    $C = \Sigma_{i,z}((x_i - \mu_{z,i})^2)$ (6)

5   where C represents the sum of the Euclidian distances between each observation (x_i) and its

6   respective cluster centre (μ_{z_i}), according to Eq. 6.

7   The number of clusters (k) that best represents the data is a critical choice in order to

8   perform a proper cluster analysis. The addition of a cluster ($k+1$) on one hand adds

9   complexity to the solution, while on the other hand decreases the cost function. A typical

10   strategy to select the right number of clusters is to explicitly penalize the addition of new

11   clusters by using Bayesian information criteria. This approach consists in adding a penalty

12   term to Eq. 6 proportional to the number of clusters (k):

13   $C' = \Sigma_{i,z}((x_i - \mu_{z,i})^2) + k \cdot ln(D)$ (7)

14   where D denotes the dimensionality of the clusters (24 in our case, as we consider diurnal

15   cycles with hourly time resolution). In this study the C' function showed the minimum at 5

16   clusters (Fig. S5). The absence of convexity properties (i.e. several local minima can exist and

17   the solution strongly depends on the initialization) represents a possible drawback of the k-

18   means algorithm, therefore 100 random initializations of the k-means algorithm were

19   conducted.

20   The best clusters are selected based on a novel statistical analysis of the HOA, COA and

21   BBOA average cluster spectra (SI). Briefly, a cluster was retained if the HOA, COA, and

22   BBOA average cluster spectra were not statistically different from the average reference

23   HOA, COA, and BBOA spectra from literature (Crippa et al., 2013b; Mohr et al., 2012; Bruns

24   et al., 2015; Docherty et al., 2011; Setyan et al., 2012; He et al., 2010, Table S3). A complete

25   description of the best clusters selection is reported in the SI (Figs. S4-S7). Overall, three

26   clusters were retained and 2 were rejected. Finally, we retained only the PMF solutions that

27   were attributed to the 3 best clusters in more than 95% of the k-means random initializations

28   (Fig. S8).

29   In order to explore the rotational ambiguity of our PMF model we performed 200 PMF runs

30   by initiating the PMF algorithm using different input matrices. The 200 different input

31   matrices were generated using a bootstrap approach (Davison and Hinkley, 1997; Brown et

32   al., 2015). In short, the bootstrap approach creates new input matrices by randomly

33   resampling mass spectra (i elements) from the original input matrices. Note that some mass

1   spectra are resampled multiple times, while others are not represented at all. On average we

2   randomly resampled 63±1% of the original spectra per bootstrap PMF run. Finally, each

3   bootstrap PMF run was initiated by randomly varying the HOA and COA a-values using the

4   {a-value HOA; a-value COA} combinations previously selected as optimal from the cluster

5   analysis (Fig. S9). Only solutions showing a higher COA diurnal correlation with the three

6   selected clusters than with the two rejected clusters were retained. In this way we rejected

7   3.7% of the solutions. In the following we present the average bootstrap solution. The source

8   apportionment uncertainty is calculated as the variability of the retained bootstrap PMF runs.

10 *Offline-AMS source apportionment optimization.*

11 In this section we discuss the optimization of the offline-AMS source apportionment. The

12 PMF input matrices included 217 ions and 538 time elements deriving from about 10 AMS

13 mass spectral repetitions collected for each of the 54 composite samples.

14 Based on analysis of the PMF residuals, we selected a 5-factor solution to explain the

15 variability of our dataset (Fig. S10). Similar to online-AMS, we monitored the decrease in

16 Q/Q_{exp} when increasing the number of factors (z). In this study, a large Q/Q_{exp} decrease was

17 observed until 5 factors. We also observed a clear $\Delta Q/Q_{exp}$ structure removal until 5 factors,

18 with higher order solutions leading to additional factors that were not attributable to specific

19 aerosol sources/processes. The 5 separated factors included HOA, COA, BBOA, OOA, and

20 industry-related OA (INDOA). The complete validation of the PMF factors will be discussed

21 in the Results section.

22 To explore the rotational ambiguity of our PMF model we performed 1080 bootstrapped PMF

23 runs. In this case we performed a higher number of bootstrap runs than online-AMS because

24 the COA and HOA a-value combinations could not be separately optimized because the

25 offline-AMS method cannot resolve diurnal patterns. Each PMF run was also initiated using

26 different input matrices. As previously mentioned the input matrices contained about 10 mass

27 spectral repetitions per filter sample, therefore the bootstrap algorithm was implemented to

28 randomly resample 54 filters samples, each one with all the corresponding mass spectral

29 repetitions. The final generated matrices included 54 samples; note that some filter samples

30 could be resampled more times, while others were not resampled at all. On average 63±5% of

31 the original samples were resampled. Finally, each of the PMF runs was initiated by randomly

1 varying the HOA and COA *a*-values. The optimal PMF solutions were selected based on 6

2 acceptance criteria including:

    1) Significantly (*p*=0.05) positive Pearson correlation coefficient *R* between BBOA and levoglucosan.

    2) Significantly positive *R* between HOA and NO_x.

    3) Significantly positive *R* between INDOA and Se.

    4) BBOA correlation with levoglucosan (*R*) significantly higher than the correlation between COA and levoglucosan.

    5) HOA correlation with NO_x significantly higher than the correlation between COA and NO_x.

    6) COA correlation with Se significantly smaller than the correlation between INDOA and Se.

13 Criteria 1-3 analyse the correlation between factor and marker time series. The significance of

14 a correlation was determined by calculating the Fisher transformed correlation coefficient *z*

15 (Garcia, 2011):

$$z = 0.5 * \ln\left(\frac{1+R}{1-R}\right) = \arctan(R) \tag{8}$$

17 where *R* is the Pearson correlation coefficient between factor and marker time series.

18 Subsequently we conducted a *t*-test to verify the significance (*α*=0.95) of the correlation:

$$t = \frac{R}{\sqrt{\frac{1-R^2}{N-2}}} \tag{9}$$

20 Here, *N* represents the number of samples (54). For a confidence interval of 95% the

21 minimum significant correlation was *R* = 0.23. For criteria 4-6, in order to evaluate whether

22 HOA, BBOA and INDOA correlated significantly better than COA with their corresponding

23 markers, we compared the *z* values obtained between each factor and its corresponding tracer

24 (e.g. BBOA and levoglucosan) and between COA and the same tracer (e.g. levoglucosan),

25 using a standard error on the *z* distribution of $1/\sqrt{N-3}$ (Zar, 1999).

26 In total, we retained 1.5% of the PMF runs. The criteria that discarded the largest number of

27 solutions were the ones based on COA (4-6) correlation with tracers of other sources. This

28 suggests that for this dataset the COA separation from other sources was particularly difficult

29 due to the absence of high temporal resolved data which aids the separation of a distinct COA

1   diurnal cycle. Moreover, this separation is also complicated by the small COA contribution

2   estimated by both online- and offline-AMS source apportionments (on average 0.4 μg m^{-3} as

3   discussed in the following sections). Furthermore, the relatively small R_{COA} (median 0.54)

4   hampers the COA apportionment by offline-AMS.

5   The PMF performed on offline-AMS mass spectra returned water-soluble OA factor

6   concentrations, KOA_i. To rescale the water-soluble OA concentration to the total OA,

7   $WSKOA_i$, we used the factor recoveries (R_k) reported by Daellenbach et al. (2016) for the

8   HOA, COA, BBOA, and OOA factors (R_{HOA}, R_{COA}, R_{BBOA}, R_{OOA}).

9   $KOA_i = WSKOA_i/R_{KOA}$ (10)

10 This is the first offline-AMS study where an INDOA factor was identified. Therefore, we

11 determined the INDOA recovery (R_{INDOA}) in this study, by performing a single parameter fit

12 according to Eq. 11:

13 $OC_i = \dfrac{WSHOA_i}{\frac{OM}{OC}_{HOA} \cdot R_{HOA}} + \dfrac{WSCOA_i}{\frac{OM}{OC}_{COA} \cdot R_{COA}} + \dfrac{WSBBOA_i}{\frac{OM}{OC}_{BBOA} \cdot R_{BBOA}} + \dfrac{WSOOA_i}{\frac{OM}{OC}_{OOA} \cdot R_{OOA}} + \dfrac{WSINDOA_i}{\frac{OM}{OC}_{INDOA} \cdot R_{INDOA}}$.   (11)

14 500 different fits were performed for each of the retained PMF solutions. Moreover each fit

15 was initiated using different R_{KOA} combinations randomly selected from the R_{KOA}

16 combinations determined by Daellenbach et al. (2016) and reported in Bozzetti et al. (2016a).

17 In order to account for possible WSOC and OC systematic measurement biases, each fit was

18 initiated by also perturbing the OC_i, $WSKOA_i$, and R_{KOA} inputs assuming for each parameter a

19 possible bias of 5%, corresponding to the WSOC and OC measurement accuracy. Finally the

20 input OC_i was randomly perturbed within its measurement uncertainty assuming a normal

21 distribution of the errors. Among the performed fits we retained the recovery combinations

22 and factor time series associated with OC_i unbiased residuals (residual distribution centered

23 on 0 within the 1st and 3rd quartiles) for all seasons together and for summer and winter

24 separately (Fig. S11). Accordingly, we retained 13% of the solutions. All the retained factor

25 recovery combinations can be found at http://doi.org/10.5905/ethz-1007-75. The median

26 INDOA recoveries were estimated as 0.69 (1st quartile 0.65, 3rd quartile 0.73, Fig. S12), while

27 the retained R_{KOA} for the other sources were consistent within the quartiles with the R_{KOA}

28 values reported by Daellenbach et al. (2016) despite their input value was perturbed as

29 described above. The variability of the retained solutions is considered as our best estimate of

30 the source apportionment uncertainty, which accounts for offline-AMS repeatability, model

31 rotational uncertainty explored bootstrapping the input matrices and scanning the HOA and

1   COA a-value sensitivity, and R_{KOA} uncertainties. Overall, for a generic factor KOA, we

2   estimated the corresponding average relative uncertainty as follows: we calculated the

3   campaign averages of the KOA concentrations for each of the v retained PMF solutions

4   ($\overline{KOA_v}$). The relative uncertainty of the KOA concentration was calculated as the standard

5   deviation of $\overline{KOA_v}$ divided by its average.

6   We also explored a 4-factor solution without constraining the COA profile. In this case we

7   performed 100 bootstrap PMF runs by randomly varying the HOA a-value. Results revealed

8   the COA separation (in the 5-factor solution with COA constrained) affected the HOA

9   separation more than the other factors (BBOA, OOA, INDOA). Overall, when comparing the

10   4- and 5-factor solutions (without and with COA constrained, respectively) HOA showed not

11   statistically different concentrations within our estimated source apportionment uncertainty

12   for 85% of the samples, BBOA and OOA for 96%, and INDOA for 94%. This is probably due

13   to the high similarity between COA and HOA spectra (SI, "Best cluster selection" Section),

14   which are both characterized by high contributions from hydrocarbons.

3   Source apportionment validation

17   Figure 1 displays the stacked seasonal average concentrations of the measured $PM_{2.5}$

18   components (ions measured by IC, elements measured by ICP-MS, EC by the EUSAAR

19   method, and OM estimated as the sum of the offline-AMS PMF factors). Higher

20   concentrations were observed during winter than in summer due to the enhanced contributions

21   of NO_3^- and OM. NO_3^- increased during winter and autumn due to NH_4NO_3 partitioning into

22   the particle phase at lower temperatures. OM concentrations were higher during winter due to

23   the strong BBOA contributions.

24   Overall OM was the dominant $PM_{2.5}$ component over the whole year highlighting the

25   importance of studying its sources. OM represented 46% of the total mass with higher relative

26   contributions during winter (51%) than in summer (37%). SO_4^{2-} represented the second most

27   abundant $PM_{2.5}$ component, contributing on average 12% of the mass. Among the other

28   components, EC contributed 9% of the mass, NO_3^- 9% ($13\%_{avg}$ during winter and $3\%_{avg}$

29   during summer), NH_4^+ 8%, the sum of the elements 7% (3% during winter and 13% during

30   summer, possibly because of dust resuspension), CO_3^{2-} 6%, Ca^{2+} 2%. K^+, Cl^-, Na^+, and Mg^{2+}

1   individually did not exceed 1% of the mass. In the following, subscripts *avg*, and *med* denote

2   average and median values, respectively.

3   **3.1 Online-AMS source apportionment validation**

4   PMF factors were associated to aerosol sources/processes based on mass spectral features

5   (Fig. 2), correlation with tracers (Fig. 3), and diurnal cycles (Fig. 4). The HOA was well-

6   correlated with NO_x (R=0.86), with peaks during rush hours (centered on 8h and 19h) and

7   higher concentrations during the first half of the campaign. The average HOA/NO_x ratio (µg

8   m^{-3}/µg m^{-3}) was 0.024, consistent with Favez et al. (2010). The COA diurnal variation showed

9   two peaks at lunch and dinner time (12.00 and 21.00), as observed in other cities (Elser et al.,

10   2016; Mohr et al., 2012). The BBOA factor profile showed the highest $fC_2H_4O_2^+$ and

11    $fC_3H_5O_2^+$ contributions among the apportioned factors. Previous studies (Alfarra et al., 2007)

12   associated the high $fC_2H_4O_2^+$ and $fC_3H_5O_2^+$ contributions in BBOA AMS spectra to the

13   fragmentation of anhydrous sugars from cellulose pyrolysis. The BBOA time series was well-

14   correlated with levoglucosan (R=0.74) and AMS-PAHs (R=0.88). Note that AMS-PAHs are

15   not unique BBOA tracers, but in general they derive from combustion sources. In this specific

16   dataset they could partially derive from traffic, although from the AMS-PAHs multilinear

17   regression, we estimated that 79% of the AMS-PAHs are related to BBOA and 21% to HOA,

18   indicating that BBOA dominates the PAH emissions. The AMS-PAHs:HOA ratio was

19   0.0020, while the AMS-PAHs:BBOA was 0.0028. In general, industrial emissions can be an

20   important source of PAHs at this location as discussed in El Haddad et al. (2013). In presence

21   of an industrial contribution, the BBOA *vs*. AMS-PAHs correlation would decrease. In this

22   work the correlation between AMS-PAHs and the $C_2H_4O_2^+$ fragment, typically related to

23   levoglucosan fragmentation (Alfarra et al., 2007), was high (R=0.87) and no AMS-PAHs

24   spike was observed without a simultaneous increase of $C_2H_4O_2^+$ (Fig. S14). Moreover the

25   industrial-related OA factor resolved by El Haddad et al. (2013) was clearly associated to

26   wind directions from W/SW (225°-270°), while in this work wind directions were oriented

27   from W/SW only for 7% of the monitoring time, furthermore without being associated to any

28   significant increase in the AMS-PAHs concentration (Fig. S15), indicating the absence of

29   clear industrial episodes. The BBOA diurnal cycle, similarly to AMS-PAHs, showed higher

30   values at night than during the day (Fig. 4). In addition, the BBOA highest concentrations

31   were detected at night and associated to slow wind speeds from the E/NE which is consistent

32   with the night land breeze direction. Moreover, strong enhancements of the BBOA factor

1 concentrations were perceived when the wind direction shifted to the E/NE (typically around

2 18 o'clock during the monitoring period) suggesting that BBOA could be transported from

3 the valleys nearby Marseille (Fig. S17). We calculated the BBOC time series by dividing the

4 BBOA concentrations by the OM:OC$_{BBOA}$ ratio calculated from the average BBOA HR

5 spectrum (1.60). The average BBOC:levoglucosan ratio [µg m^{-3}/µg m^{-3}] was 0.15,

6 comparable to other European studies (Zotter et al., 2014; Herich et al., 2014; Minguillón et

7 al., 2011).

8 The OOA profile showed the most oxidized mass spectral fingerprint with an O:C ratio of

9 0.67 in comparison to the values of 0.35 retrieved for BBOA, 0.12 for COA and 0.03 for

10 HOA. The OOA time series was well correlated with the NH$_4^+$ time series (R=0.86),

11 suggesting a probable secondary origin of the OOA factor (Lanz et al., 2008). The OOA

12 diurnal cycle was flat, suggesting OOA to be representative of regionally-transported

13 oxygenated aerosols, consistent with the conclusions of El Haddad et al. (2013).

14 **3.2 Offline-AMS source apportionment validation**

15 PMF factors from the offline-AMS dataset were related to aerosol sources/processes based on

16 mass spectral features (Fig. 5), seasonal trends and correlation with tracers (Fig. 6). A

17 comparison of the online-AMS and offline-AMS factor profiles is reported in the SI. In the

18 following, for a generic k factor, we calculated the corresponding KOC$_i$ time series dividing

19 KOA$_i$ by the OM:OC ratio determined from the average HR-AMS factor profile.

20 During summer, when biomass burning contributions to EC are low, HOA correlated well

21 with EC (R = 0.76) and yielded an HOC:EC (Hydrocarbon-like OC = HOA/(OM:OC)$_{HOA}$)

22 ratio of 0.64, similar to other European studies (El Haddad et al., 2009 and references

23 therein). Over the whole year, the retained PMF solutions showed an HOA correlation with

24 NO$_x$ (R) spanning between 0.23 and 0.49. These low correlations are comparable to the ones

25 found by El Haddad et al. (2013) at the same station by online-AMS. In this case, the

26 relatively low HOA correlation with NO$_x$ is probably due to the low R_{HOA} (median 0.11)

27 which together with the low HOA concentration (1.5 µg m$^{-3}_{avg}$, Results section), results in

28 small water-soluble HOA concentrations, leading to an uncertain HOA apportionment. This

29 was already reported in previous offline-AMS studies (Daellenbach et al., 2016; Bozzetti et

30 al., 2016a). Although the HOA variability could not be well captured, the estimated HOA

1   concentration was corroborated by the average HOA/NO$_x$ (0.02 µg m^{-3}/µg m^{-3}) which was

2   found to be consistent with El Haddad et al. (2013) for the same station and with Favez et al.

3   (2010) for an alpine location in France.

4   BBOA was identified from its mass spectral features, with the highest $fC_2H_4O_2^+$ and $fC_3H_5O_2^+$

5   contributions among the apportioned factors, consistent with the findings of Alfarra et al.

6   (2007). BBOA correlated well with the biomass combustion tracers levoglucosan (R=0.76)

7   and vanillic acid (R=0.84). The winter average levoglucosan:BBOC [µg m^{-3}/µg m^{-3}] ratio was

8   equal to 0.12, consistent with other studies in Europe (Zotter et al., 2014; Herich et al., 2014;

9   Minguillón et al., 2011).

10   The fourth factor (INDOA) was related to industrial emissions due to the high correlation

11   with light alkanes (C19-C22, 0.77≤R≤0.86), Se (R=0.54), Pb (R=0.44) and with some PAHs

12   such as pyrene (R=0.74), fluoranthene (R=0.77), and phenantrene (R=0.74). Among the

13   measured PAHs, pyrene, fluoranthene and phenantrene showed the lowest correlations with

14   levoglucosan (Table S1, R = 0.31, 0.29, and 0.27 respectively), suggesting that these

15   particular PAHs were overwhelmingly emitted by INDOA rather than BBOA. While Se is

16   considered to be a unique coal marker in the literature (Weitkamp et al., 2005; Park et al.,

17   2014), in Marseille this source is likely related to coke and steel production facilities (El

18   Haddad et al., 2011). The average INDOA OM:OC (1.60) was intermediate between the

19   OM:OC ratios of HOA (1.23) and COA (1.28), and those of BBOA (1.85) and OOA (1.82).

20   El Haddad et al. (2013) resolved an industrial OA factor at the same station by online-AMS

21   PMF. In that work the authors suggested a probable contribution of oxygenated OA to the

22   resolved industrial factor, probably deriving from (photo)chemical aging during the transport

23   from the industrial facilities to the receptor site occasionally accompanied by new particle

24   formation processes within the industrial plume (as observed by the increased ultrafine

25   particle number concentration associated to W/SW wind directions) . Considering the average

26   wind speed from W/SW (0.8 km/h), and the distance between the receptor site and the

27   Marseille commercial harbor (~ 40 km) we estimate an aging time of several hours, which

28   could lead to a more oxidized fingerprint in comparison to the fresh primary emissions

29   (Huang et al., 2014). Overall this factor explained the largest fraction of the variability of S-

30   and Cl-containing organic fragments such as C_2HSO^+, CH_2SO^+, $CH_3Cl_2^+$, $CH_4SO_3^+$,

31    $C_3H_3SO_2^+$, and $C_7H_{16}^+$.

1 The last factor was defined as OOA as it showed a highly oxygenated fingerprint with the

2 largest CO_2^+ fractional contributions (fCO_2^+) among the apportioned factors (14%, in

3 comparison with 11% for BBOA, 2% for HOA, and 1% for COA and INDOA). This factor

4 showed on average the largest contributions over the year. Overall, the OOA:NH_4^+ ratio was

5 2.3_{avg}, in line with the values reported by Crippa et al. (2014) for 25 different European sites

6 (2.0_{avg}; minimum value 0.3; maximum 7.3).

7 Previous offline-AMS (Bozzetti et al., 2016a; Bozzetti et al., 2016b; Daellenbach et al., 2016)

8 and online-ACSM studies (e.g., Canonaco et al., 2015) conducted in Switzerland and

9 Lithuania reported the separation of two OOA factors characterized by different seasonal

10 trends and different $C_2H_3O^+$:CO_2^+ ratios. In particular, the OOA factor characterized by the

11 highest $C_2H_3O^+$:CO_2^+ ratio contributed mostly during summer and was linked to secondary

12 OA from biogenic emissions. Here we calculated a $(C_2H_3O^+$:$CO_2^+)_{OOA}$ ratio by subtracting the

13 $C_2H_3O^+$ and CO_2^+ contributions deriving from primary sources, from the measured $C_2H_3O^+$

14 and CO_2^+ (Canonaco et al., 2015):

$$\frac{C_2H_3O^+}{CO_2^+}_{OOA,i} = \frac{C_2H_3O^+_{meas,i} - HOA_i \cdot fC_2H_3O^+_{HOA} - BBOA_i \cdot fC_2H_3O^+_{BBOA} - INDOA_i \cdot fC_2H_3O^+_{INDOA} - COA_i \cdot fC_2H_3O^+_{COA}}{CO_2^+_{meas,i} - HOA_i \cdot fCO_2^+_{HOA} - BBOA_i \cdot fCO_2^+_{BBOA} - INDOA_i \cdot fCO_2^+_{INDOA} - COA_i \cdot fCO_2^+_{COA}} \quad (12)$$

16 Overall, $C_2H_3O^+_{OOA}$, and $CO_2^+_{OOA}$ did not show a clear seasonality, which hampered the

17 separation of two OOA sources. Even though another OOA factor was not separated, El

18 Haddad et al. (2013) estimated for the same location during summer a substantial contribution

19 of secondary biogenic aerosol using ^{14}C measurements (no measurements conducted in other

20 seasons). As a consequence the OOA factor resolved in this work explains both secondary

21 biogenic and aged/secondary anthropogenic sources. The absence of a clear increase in the

22 $(C_2H_3O^+$:$CO_2^+)_{OOA}$ ratio in Marseille during summer could be explained by the large

23 emissions of anthropogenic secondary OA (SOA) precursors during winter, leading to a

24 different $(C_2H_3O^+$:$CO_2^+)_{OOA}$ seasonality in comparison with previous offline-AMS studies

25 (Daellenbach et al., 2016, Bozzetti et al. 2016a), which were conducted either at rural sites

26 characterized by different types of vegetation, or in smaller urban areas. In general, several

27 parameters affect the biogenic SOA concentrations and their separation, e.g. intensity of the

28 biogenic precursor sources, air masses photochemical age, and NO_x concentrations. . All

29 those parameters were different in Marseille from previous offline-AMS studies which were

30 conducted in central/northern Europe.

1   **4. Results and discussion**

2   **4.1 OA source apportionment results and uncertainties.**

3   In this study, we present one the first OA source apportionments conducted over an entire

4   year in the Mediterranean region and the first comparison between HR online-AMS and

5   offline-AMS source apportionments, as Daellenbach et al. (2016) compared offline-AMS

6   results to online ACSM data in Zurich. Although related to different years and size-fractions

7   (PM_1 online-AMS, $PM_{2.5}$ offline-AMS), the offline-AMS source apportionment returned

8   average seasonal factor concentrations not statistically different to online-AMS for both

9   winter (Fig. 7) and summer (comparison with El Haddad et al., 2013, Fig. 8). We note that the

10   total OC concentration quantified by online-AMS for PM_1 and by the thermal-optical

11   procedure used for the offline-AMS source apportionment of $PM_{2.5}$ was not different on a

12   seasonal scale considering our uncertainty which includes time variability and measurements

13   uncertainties.

14   Both online and offline-AMS source apportionment revealed that BBOA was the largest OA

15   source during winter. Offline-AMS source apportionment estimated an average BBOA

16   concentration during winter 2011-2012 of 5.2 $\mu g\ m^{-3}_{avg}$, representing $43\%_{avg}$ of the OA.

17   Similarly, online-AMS source apportionment revealed a BBOA concentration of $4.4_{avg}\ \mu g\ m^{-3}$

18   (corresponding to 42% of OA) during February 2011. During summer, the offline-AMS

19   BBOA concentration dropped to an average of 0.3 $\mu g\ m^{-3}_{avg}$ representing 5% of the OA. Not

20   surprisingly such low BBOA contributions were not resolved by online-AMS source

21   apportionment during summer (El Haddad et al., 2013). On average the offline-AMS BBOA

22   relative uncertainty was 9%. As a comparison, the online-AMS BBOA average relative

23   uncertainty was 6%. Overall for both online- and offline-AMS, the BBOA contributions were

24   the least uncertain among the primary sources, possibly because of the high loadings and the

25   distinct seasonal and diurnal BBOA variability in comparison with the other separated factors.

26   A comparison between the offline- and online-AMS source apportionment uncertainties can

27   be carried out with the caveat that the online-AMS source apportionment uncertainties

28   estimated in this work should be considered as a low estimate as they do not account for the

29   AMS mass error deriving mostly from CE, and particle transmission. This source of

30   uncertainty affects the total OA mass but not the relative contribution of the factors. By

31   contrast, the OA mass uncertainty was accounted for in the offline-AMS source

1   apportionment as the OA mass was rescaled to external measurements (WSOC and OC), the

2   uncertainty of which was propagated in the final source apportionment error (Section 2.4).

3   On a yearly scale, the offline-AMS source apportionment revealed that OOA was the largest

4   OA source, with the highest relative contributions during summer due to the reduced BBOA

5   emissions. The OOA concentration during summer was estimated from offline-AMS at 3.0 μg

6   m$^{-3}_{avg}$, corresponding to 55% of the OA mass. El Haddad et al. (2013) also reported OOA to

7   be the dominant OA fraction during summer with a similar average concentration of 2.9 μg m^{-}

8   ^{3}. During winter, the OOA concentration was estimated by online-AMS to be 3.9$_{avg}$ μg m^{-3}

9   corresponding to 38% of the OA, while the OOA relative uncertainty was 4%. As a

10   comparison, the OOA relative uncertainty from offline-AMS was 6%$_{avg}$. The offline-AMS

11   source apportionment revealed similar OOA concentrations during winter (3.4 μg m$^{-3}_{avg}$

12   corresponding to 27%$_{avg}$ of the OA). Even though during winter the OOA concentration was

13   higher than in summer, possibly due to partitioning and due to the shallower boundary layer,

14   the relative contribution decreased because of the strong BBOA contributions.

15   HOA is one of the most uncertain factors, with an average relative uncertainty of 39%

16   estimated from offline-AMS and 10% from online-AMS analysis, where the larger

17   uncertainty observed for offline-AMS derives mostly from the low R_{HOA} and from the lower

18   time resolution which does not capture the traffic diurnal variability. On average, the HOA

19   concentration predicted by offline-AMS was 1.5 μg m^{-3}, corresponding to 17% of the OA.

20   The estimated HOA concentration by online-AMS during February 2011 was 1.6 μg m$^{-3}_{avg}$

21   (16% of OA). These values are higher than the ones of El Haddad et al. (2013) who estimated

22   a traffic contribution of 0.8 μg m$^{-3}_{avg}$ during July 2008.

23   The COA contributions were only minor (average of 0.3 μg m^{-3}), representing on average 4%

24   of the OA mass according to the offline-AMS source apportionment. The online-AMS winter

25   source apportionment returned similar concentrations with 0.4 μg m$^{-3}_{avg}$, equivalent to 4%$_{avg}$

26   of the OA. Overall, due to the low concentrations, the COA contributions were uncertain in

27   both source apportionments (6% for online-AMS, 73% for offline-AMS).Similarly to HOA,

28   the larger uncertainty observed for offline-AMS was most possibly due to the low $R_{COA,}$ and

29   the low time resolution which did not enable the COA separation based on the diurnal

30   variability. The summer COA contribution was not resolved from HOA by El Haddad et al.

31   (2013), possibly because the COA reference mass spectrum was not constrained and because

32   of the lack of HR data which typically aid the separation of the two sources.

1   Finally, the INDOA factor concentration estimated from offline-AMS was on average 2.1 μg

2   m^{-3} during winter and 0.6 μg m$^{-3}_{avg}$ during summer, where this seasonal trend was driven by a

3   strong episode that occurred during early February. The offline-AMS relative uncertainty was

4   estimated as 17%. As previously discussed, this factor was not separated by online-AMS

5   analysis (February 2011) because of the absence of clear events, which in the offline-AMS

6   dataset were observed only over a short period during January-February 2012. An industrial

7   factor was instead resolved by El Haddad et al. (2013) during summer 2008, with an average

8   concentration of 0.3 μg m$^{-3}_{avg}$. In that study, the industrial OA factor was also characterized

9   by a low background intercepted by ten-fold spiking episodes.

10   From the sum of the offline-AMS factor concentrations we estimated the total OM mass.

11   Using this OM and the measured OC we calculated the OM:OC ratio to be 1.40 on average.

12   Specifically, during winter this ratio was 1.55, which is consistent with the online-AMS

13   values determined from the HR-AMS spectra (median = 1.52, 1st quartile = 1.46; 3rd quartile

14   1.59). The bulk OM:OC variability was driven by the source variabilities. Indeed the relative

15   contribution of the most oxidized source (OOA) was higher during summer (mostly due to the

16   absence of BBOA), however also the relative contributions of the less oxidized sources (such

17   as HOA and COA) were higher during summer mostly due to low BBOA contributions. The

18   BBOA mass spectrum instead was associated with intermediate OM:OC ratios comprised

19   between the values of COA and OOA, and therefore influenced less strongly the bulk OM:OC

20   ratio. Overall the combination of these effects led to a higher bulk OM:OC during winter.

4.2 Insights into the BBOA origin during winter

23   Methyl-nitrocatechols measurements showed high correlations with BBOA (Fig. 9, R=0.95)

24   and no correlation with OOA (R=0.06, offline-AMS source apportionment). Similarly high

25   correlations were already observed in other studies (e.g. Poulain et al., 2011). This large

26   correlation difference suggests that the variability of the methyl-nitrocatechols is likely

27   explained by the BBOA source. However, methyl-nitrocatechols are secondary compounds

28   deriving from the nitration of catechols which can be either directly emitted by wood

29   combustion (Schauer et al., 2001), or generated by OH· oxidation of cresols directly released

30   by wood combustion (Iinuma et al., 2010). m-cresol/NO$_x$ photooxidation experiments (Iinuma

31   et al., 2010) revealed a total contribution of all methyl-nitrocatechol isomers to the catechol

1   SOA of approximately 10%. Assuming that methyl-nitrocatechols are apportioned entirely to

2   the BBOA factor, we estimate a methyl-nitrocatechol-SOA contribution to BBOA on the

3   order of 8%, indicating that part of the BBOA factor is of secondary origin. Previous studies

4   (Atkinson and Arey, 2003) revealed an o-cresol life-time in the atmosphere of 2.4 minutes

5   towards NO_3, and 3.4 h towards OH (at 298 K, dark conditions). This would suggest that such

6   fast SOA formation can be better traced by the high time resolution online-AMS source

7   apportionment (8 minutes) than by the offline-AMS with 24 h time resolution, and in any case

8   only in the BB plume or in the vicinity of the emission source. Nevertheless we did not

9   observe statistically different ratios (within 1σ, error calculated as the time variability) of

10   $OOA:NH_4^+$ (1.5_{avg} and 1.25_{avg} for the offline-AMS and online-AMS source apportionments,

11   respectively), OOA:BBOA (0.65_{avg} and 0.89_{avg} respectively), and levoglucosan:BBOC

12   (1.13_{avg} and 1.15_{avg} respectively, Fig. 10) during winter, suggesting that despite the different

13   time resolutions, the online and offline methods provide a comparable BBOA-SOA

14   separation.

15   Both online- and offline-AMS source apportionment revealed for the two different winter

16   seasons a comparable temporal evolution of the levoglucosan:BBOC ratio (Fig. 10, and Fig.

17   11). This ratio showed typical literature values for domestic wood combustion in Europe

18   during January and early February (0.05-0.2, Zotter et al., 2014; Herich et al., 2014;

19   Minguillón et al., 2011), while during late autumn and March (Fig. 11) it increased up to 0.3,

20   highlighting an evolution of the BBOA chemical composition. A similar seasonal trend was

21   observed for the levoglucosan:vanillic acid, levoglucosan:syringic acid, and levoglucosan:non

22   sea salt-K^+ (nss-K^+, calculated according to Seinfeld and Pandis, 2006) ratios (Fig. 11).

23   Although the online dataset was limited to one month of measurements, the

24   levoglucosan:vanillic acid ratio also showed a statistically significant increasing trend from

25   early February to the beginning of March (confidence interval of 95%, Mann-Kendall test).

26   These results suggest the occurrence of different types of biomass combustions during low

27   temperature winter days compared to late autumn and early spring: as levoglucosan derives

28   from cellulose pyrolysis (>300°C), while vanillic and syringic acid result from lignin

29   combustion (Simoneit et al., 1998, Sullivan et al., 2008). Different reactivities / volatilities of

30   BBOA markers may complicate this analysis. For this reason we discuss in the following the

31   levoglucosan stability, and propose that the major driver of the observed seasonal trends is the

32   occurrence of different BBOA combustions.

1 Previous studies revealed the levoglucosan reactivity toward OH· radical oxidation (Hennigan

2 et al., 2010) both in gas and aqueous phase (Hoffmann et al., 2010). In the following we

3 analyze the levoglugocan and nss-K^+ time series in order to investigate the possible effects of

4 levoglucosan chemical stability and different types of biomass combustions on the seasonal

5 evolution of the levoglucosan:nss-K^+ ratio. During summer nss-K^+ derives mostly from dust,

6 while levoglucosan is depleted by both photochemistry (Hennigan et al., 2010) and low

7 BBOA emissions. Not surprisingly the levoglucosan:nss-K^+ ratio showed lower values in

8 summer (0.25) than in winter (3.35). During winter nss-K^+ is considered to be mostly emitted

9 by BBOA, and consistently in our dataset it shows a good correlation with BBOA tracers

10 (R=0.66 with syringic acid). Overall, the levoglucosan:nss-K^+ ratio during the cold season

11 manifests a behavior that is opposite to the photochemical activity (with temperature

12 considered as a proxy) as it shows higher values during March and late autumn (up to 15.7)

13 and lower in January February (minimum = 6.3; Fig. 11) when temperature is lower and

14 photochemistry is less intense. For these reasons we relate the winter levoglucosan:nss-K^+

15 variability to different types of combustion rather than to a levoglucosan depletion due to

16 photochemistry. Furthermore we observed the highest levoglucosan concentrations (late

17 autumn) simultaneously with the highest relative humidity (89%) values, suggesting the

18 depletion of levoglucosan by OH· radical oxidation in aqueous phase to be not significant

19 (Hoffmann et al., 2010).

20 A similar winter seasonal behavior was observed also for plant waxes. Plant waxes

21 concentrations were estimated from high molecular weight n-alkanes (C24-C35) according to

22 the methodology described by Li et al. (2010). This methodology is based on the observation

23 that alkanes from epicuticular waxes preferentially contain an odd number of carbon atoms

24 (Aceves and Grimalt, 1993; Simoneit et al., 1991). This was observed for a large variety of

25 plants including broad leaf trees, conifers, palms, shrubs, grasses, and groundcover

26 (Hildemann et al., 1996 and references therein). Waxes showed the highest concentrations

27 during late autumn (up to 0.16 µg m^{-3}) and in May (up to 0.17 µg m^{-3}), while the minima were

28 observed during winter (minimum 0.007 µg m^{-3}). In general, high molecular weight n-alkanes

29 are typically detected in atmospheric aerosol in significant amounts during the growing

30 season. In a similar way, Hildemann et al. (1996) estimated the highest plant waxes

31 concentrations in April-May in Los Angeles and Pasadena where the climate is similar to

32 Marseille. Similarly we observed the highest concentrations during May. However,

33 comparable plant waxes concentrations were observed also in late autumn during the period

1   characterized by the highest levoglucosan:lignin combustion tracers (Fig 11), suggesting a

2   possible emission from open combustion of green wastes.

3   Taken together the above observations suggest the occurrence of combustion of cellulose-rich

4   material during March and late autumn, compared to lignin rich biomass burning for

5   residential heating during January. The combustion of cellulose-rich material is possibly

6   related to agricultural waste burning at the beginning and at the end of the agricultural cycle.

7   The occurrence of emission of biomass plumes due to land clearing episodes during March

8   has already been reported in other parts of Europe (Ulevicius et al., 2016), and has been

9   previously modelled for southern France (Dernier van der Gon et al., 2015, Fountoukis et al.,

10   2014).

11   We note that BB is described in our PMF models by only one factor which therefore

12   potentially represents a combination of several types of biomass burning sources. Increasing

13   the number of factors did not lead to an unambiguous separation of different BBOA sources,

14   however, the comparison with source-specific markers revealed a real BBOA composition

15   evolution over the winter season with higher cellulose to lignin combustion tracer ratios

16   observed during late autumn and early spring in comparison to January/February. This

17   hypothesis of at least two types of BB sources (one linked to domestic heating, another to

18   agricultural activities) is also supported by the direct PMF analysis of the organic and

19   inorganic markers measured for batch 1 (Salameh et al., *in prep.*).

21   **5   Conclusions**

22    $PM_{2.5}$ filter samples were collected during an entire year (August 2011 to July 2012) at an

23   urban site in Marseille, France. Filter samples were analyzed by water extraction followed by

24   nebulization of the liquid extracts and subsequent measurement of the generated aerosol with

25   an HR-ToF-AMS (Daellenbach et al., 2016).

26   PMF analysis was conducted on the offline-AMS mass spectra and on online-AMS data

27   collected at the same station during February 2011. Offline-AMS source apportionment

28   results were also compared with a previous online-AMS source apportionment study of two

29   weeks during July 2008 at the same location (El Haddad et al., 2013). The methods returned

30   statistically similar seasonal factor concentrations, although different years and size fractions

31   were considered (PM_1 for online-AMS, $PM_{2.5}$ for offline-AMS). OOA was the major source

1   of OA during summer representing on average 55% of the OA mass, while BBOA was the

2   dominant OA source during winter contributing on average 43% of the OA. Smaller

3   contributions were estimated for HOA, INDOA and COA, representing 17%, 12%, and 4% of

4   the OA mass, respectively. The contribution of primary anthropogenic sources (HOA +

5   BBOA + COA + INDOA) was substantial over the year ($62\%_{avg}$ of OA), with larger absolute

6   and relative contributions during winter (73% of OA_{avg}) associated with an intense biomass

7   burning activity.

8   Coupling offline- and online-AMS data with molecular markers showed increasing

9   levoglucosan:BBOC ratios during the late winter-early spring period in both 2011 and 2012.

10 This trend was also observed for the ratios between cellulose and lignin combustion markers

11 (e.g. levoglucosan:vanillic acid), with ratios approaching more typical domestic wood

12 combustion European values during January/early February, and values characterized by

13 higher values of cellulose-combustion markers during late autumn and March indicative of

14 the influence of different types of fuels, possibly related to agricultural-related activities.

15 From the offline-AMS source apportionment, we observed a high BBOA correlation with

16 nitrocatechols deriving from the nitration of catechols directly emitted by biomass

17 combustion. These secondary components are rapidly formed in the atmosphere in presence

18 of $NO_3\cdot$ (life time of a few minutes). Overall, despite the different time resolution, online- and

19 offline-AMS provided a comparable SOA-BBOA separation during winter. Nevertheless, in

20 case of fast SOA formation (relative to the time scale of the online-AMS time resolution, or

21 relative to the transport time to the receptor site) this separation can be hindered, and further

22 efforts are needed to improve the SOA separation from BBOA.

24 **Authors contributions:**

25 Experimental design: A. S. H. Prévôt, I. El Haddad, N. Marchand, and C. Bozzetti

26 Filter collections and online-AMS measurements: N. Marchand and D. Salameh.

27 Offline-AMS analysis: C. Bozzetti, E. Müller, K. R. Daellenbach, and I. El Haddad

28 WSOC and TN analysis: P. Fermo and R. Gonzalez

29 Sunset, and IC analysis: J.-L. Jaffrezo

30 GC-MS analysis: D. Salameh, and N. Marchand

1   Nitrocatechols analysis: Y. Iinuma

2   Carbonates analysis: M. C. Minguillón

3   Data analysis and validation: C Bozzetti, and I. El Haddad

4   PMF analysis: C. Bozzetti

5   All authors read and commented on the manuscript.

7   **Acknowledgements**

8   CB thanks the Lithuanian–Swiss Cooperation Programme "Research and Development"

9   project AEROLIT (Nr. CH-3-.MM-01/08). JGS acknowledges the support of the Swiss

10   National Science Foundation (Starting Grant No. BSSGI0 155846). IE-H acknowledges the

11   support of the Swiss National Science Foundation (IZERZ0 142146). This work has also been

12   supported by the MED program (APICE, grant number 2G-MED09-026: http://www.apice-

13   project.eu/), the French Environment and Energy Management Agency (ADEME) and

14   Provence Alpes Cote d'Azur Region (PACA). Part of the OC/EC analysis carried out in MRS

15   has been supported by the French national CARA program. This program is directed by O.

16   Favez (INERIS; http://www.ineris.fr/). He is gratefully acknowledged.

References

Aceves, M. and Grimalt, J. O.: Seasonally dependent size distributions of aliphatic and polycyclic aromatic hydrocarbons in urban aerosols from densely populated areas, Environ. Sci. Technol., 27(13), 2896–2908, doi:10.1021/es00049a033, 1993.

Aiken, A. C., DeCarlo, P. F., Kroll, J. H., Worsnop, D. R., Huffmann, J. A., Docherty, K. S., Ulbrich, I. M., Mohr, C., Kimmel, J. R., Sueper, D., Sun, Y., Zhang, Q., Trimborn, A., Northway, M., Ziemann, P. J., Canagaratna, M. R., Onasch, T. B., Alfarra, M. R., Prevot, A. S. H., Dommen, J., Duplissy, J., Metzger, A., Baltensperger, U., and Jimenez J. L. O/C and OM:OC ratios of primary, secondary, and ambient organic aerosols with high-resolution time-of-flight aerosol mass spectrometry. Environ. Sci. Technol. 42, 4478-4485, 2008.

Aksoyoglu, S., Keller, J., Barmpadimos, I., Oderbolz, D., Lanz, V. A., Prévôt, A. S. H., and Baltensperger U.: Aerosol modelling in Europe with a focus on Switzerland during summer and winter episodes, Atmos. Chem. Phys., 11, 7355–7373, 2011.

Aksoyoglu, S., Keller, J., Ciarelli, G., Prévôt, A. S. H., and Baltensperger, U.: A model study on changes of European and Swiss particulate matter, ozone and nitrogen deposition between 1990 and 2020 due to the revised Gothenburg protocol, Atmos. Chem. Phys., 14, 13081-13095, doi:10.5194/acp-14-13081-2014, 2014.

Alfarra, M. R., Prévôt, A. S. H., Szidat, S., Sandradewi, J., Weimer, S., Lanz, V. A., Schreiber, D., Mohr, M., and Baltensperger, U.: Identification of the mass spectral signature of organic aerosols from wood burning emissions, Environ. Sci. Technol., 41, 5770–5777, 2007.

Allan, J. D., Jimenez, J. L., Williams, P. I., Alfarra, M. R., Bower, K. N., Jayne, J. T., Coe, H., and Worsnop, D. R.: Quantitative sampling using an Aerodyne aerosol mass spectrometer: 1. Techniques of data interpretation and error analysis, J. Geophys. Res.-Atmos., 108, 4090, 2003.

Atkinson, R., and Arey, J.: Atmospheric degradation of volatile organic compounds, Chem. Rev., 103, 4605-4638, 2003.

Baklanov, A., Schlünzen, K., Suppan, P., Baldasano, J., Brunner, D., Aksoyoglu, S., Carmichael, G., Douros, J., Flemming, J., Forkel, R., Galmarini, S., Gauss, M., Grell, G.,

1 Hirtl, M., Joffre, S., Jorba, O., Kaas, E., Kaasik, M., Kallos, G., Kong, X., Korsholm, U.,

2 Kurganskiy, A., Kushta, J., Lohmann, U., Mahura, A., Manders-Groot, A., Maurizi, A.,

3 Moussiopoulos, N., Rao, S. T., Savage, N., Seigneur, C., Sokhi, R. S., Solazzo, E.,

4 Solomos, S., Sørensen, B., Tsegas, G., Vignati, E., Vogel, B., and Zhang, Y.: Online coupled

5 regional meteorology chemistry models in Europe: current status and prospects, Atmos.

6 Chem. Phys., 14, 317-398, doi:10.5194/acp-14-317-2014, 2014.

7 Birch, M. E. and Cary, R. A.: Elemental carbon-based method for monitoring occupational

8 exposures to particulate diesel exhaust, Aerosol Sci. and Tech., 25, 221–241, 1996.

9 Bozzetti, C., Daellenbach, K., R., Hueglin, C., Fermo, P., Sciare, J., Kasper-Giebl, A., Mazar,

10 Y., Abbaszade, G., El Kazzi, M., Gonzalez, R., Shuster Meiseles, T., Flasch, M., Wolf, R.,

11 Křepelová, A., Canonaco, F., Schnelle-Kreis, J., Slowik, J. G., Zimmermann, R., Rudich, Y.,

12 Baltensperger, U., El Haddad, I., and Prévôt, A. S. H.: Size-resolved identification,

13 characterization, and quantification of primary biological organic aerosol at a European rural

14 site, Environ. Sci. Technol., 50, 3425-3434, doi:10.1021/acs.est.5b05960, 2016a.

15 Bozzetti, C., Sosedova, Y., Xiao, M., Daellenbach, K. R., Ulevicius, V., Dudoitis, V.,

16 Mordas, G., Byčenkienė, S., Plauškaitė, K., Vlachou, A., Golly, B., Chazeau, B., Besombes,

17 J.-L., Baltensperger, U., Jaffrezo, J.-L., Slowik, J. G., El Haddad, I., and Prévôt, A. S. H.:

18 Argon offline-AMS source apportionment of organic aerosol over yearly cycles for an urban,

19 rural and marine site in Northern Europe, Atmos. Chem. Phys. 17, 117–141, 2017.

20 Brown, S. G., Eberly, S., Paatero, P., and Norris, G. A., Methods for estimating uncertainty in

21 PMF solutions: Examples with ambient air and water quality data and guidance on reporting

22 PMF results, Sci. Tot. Environ. 518-519, 626-635, 2015.

23 Bruns, E. A., Krapf, M., Orasche, J., Huang, Y., Zimmermann, R., Drinovec, L., Močnik, G.,

24 El-Haddad, I., Slowik, J. G., Dommen, J., Baltensperger, U. and Prévôt, A. S. H.:

25 Characterization of primary and secondary wood combustion products generated under

26 different burner loads, Atmos. Chem. Phys., 15, 2825–2841, 2015.

27 Canagaratna, M. R., Jayne, J. T., Jimenez, J. L., Allan, J. D., Alfarra, M. R., Zhang, Q.,

28 Onasch, T. B., Drewnick, F., Coe, H., Middlebrook, A., Delia, A., Williams, L. R., Trimborn,

29 A. M., Northway, M. J., DeCarlo, P. F., Kolb, C. E., Davidovits, P. and Worsnop, D. R.:

30 Chemical and microphysical characterization of ambient aerosols with the Aerodyne aerosol

31 mass spectrometer, Mass Spectrom. Rev. 26:185-222, 2007.

1 Canonaco, F., Crippa, M., Slowik, J. G., Baltensperger, U., and Prévôt, A. S. H.: SoFi, an

2 IGOR-based interface for the efficient use of the generalized multilinear engine (ME-2) for

3 the source apportionment: ME-2 application to aerosol mass spectrometer data, Atmos. Meas.

4 Tech., 6, 3649-3661, 2013.

5 Canonaco, F., Slowik, J. G., Baltensperger, U., and Prévôt, A. S. H.: Seasonal differences in

6 oxygenated organic aerosol composition: implications for emissions sources and factor

7 analysis. Atmos. Chem. Phys. 15, 6993-7002, 2015.

8 Cavalli, F., Viana, M., Yttri, K. E., Genberg, J., and Putaud, J. P.: Toward a standardised

9 thermal-optical protocol for measuring atmospheric organic and elemental carbon: the

10 EUSAAR protocol, Atmos. Meas. Tech., 3, 79-89, 2010.

11 Chauvel, C., Bureau, S., and Poggi, C.: Comprehensive chemical and isotopic analyses of

12 basalt and sediment reference materials, Geostand. Geoanalyt. Res., 35, 125–143, doi:

13 10.1111/j.1751-908X.2010.00086.x, 2010.

14 Crippa, M., Canonaco, F., Slowik, J. G., El Haddad, I., DeCarlo, P. F., Mohr, C., Heringa, M.

15 F., Chirico, R., Marchand, N., Temime-Roussel, B., Abidi, E., Poulain, L., Wiedensohler, A.,

16 Baltensperger, U., and Prévôt, A. S. H.: Primary and secondary organic aerosol origin by

17 combined gas-particle phase source apportionment, Atmos. Chem. Phys., 13, 8411-8426,

18 doi:10.5194/acp-13-8411-2013, 2013a.

19 Crippa, M., El Haddad, I., Slowik, J. G., DeCarlo, P.F., Mohr, C., Heringa, M. F., Chirico, R.,

20 Marchand, N., L., Sciare, J., Baltensperger, U., and Prévôt, A. S. H.: Identification of marine

21 and continental aerosol sources in Paris using high resolution aerosol mass spectrometry, J.

22 Geophys. Res., 118, 1950-1963, 2013b.

23 Daellenbach, K. R., Bozzetti, C., Krepelova, A., Canonaco, F., Huang, R.-J., Wolf, R., Zotter,

24 P., Crippa, M., Slowik, J., Zhang, Y., Szidat, S., Baltensperger, U., Prévôt, A. S. H., and El

25 Haddad, I.: Characterization and source apportionment of organic aerosol using offline

26 aerosol mass spectrometry, Atmos. Meas. Tech., 9, 23-39, 2016.

27 Davison, A. C. and Hinkley, D. V.: Bootstrap Methods and Their Application, Cambridge

28 University Press, Cambridge, UK, 582 pp., 1997.

29 DeCarlo, P. F., Kimmel, J. R., Trimborn, A., Northway, M. J., Jayne, J. T., Aiken, A. C.,

30 Gonin, M., Fuhrer, K., Horvath, T., Docherty, K. S., Worsnop, D. R., and Jimenez, J. L.:

1   Field-deployable, high-resolution, time-of-flight aerosol mass spectrometer, Anal. Chem., 78,

2   8281–8289, 2006.

3   Denier van der Gon, H. A. C., Bergström, R., Fountoukis, C., Johansson, C., Pandis, S. N.,

4   Simpson, D., and Visschedijk, A. J. H.: Particulate emissions from residential wood

5   combustion in Europe – revised estimates and an evaluation, Atmos. Chem. Phys., 15, 6503-

6   6519, doi:10.5194/acp-15-6503-2015, 2015.

7   Docherty, K. S., Aiken, A. C., Huffman, J. A., Ulbrich, I. M., DeCarlo, P. F., Sueper,

8   D., Worsnop, D. R., Snyder, D. C., Peltier, R. E., Weber, R. J., Grover, B. D., Eatough, D. J.,

9   Williams, B. J., Goldstein, A. H., Ziemann, P. J., and Jimenez, J. L.: The 2005 Study of

10   organic aerosols at riverside (SOAR-1): instrumental intercomparisons and fine particle

11   composition, Atmos. Chem. Phys., 11, 12387-12420, 2011.

12   Dockery, D. W., Luttmann-Gibson, H., Rich, D. Q., Link, M. S., Mittleman, M. A., Gold, D.

13   R., Koutrakis, P., Schwartz, J. D., and Verrier, R. L.: Association of air pollution with

14   increased incidence of ventricular tachyarrhythmias recorded by implanted cardioverter

15   defibrillators, Environ. Health Perspect. 113, 670-674, 2005.

16   Drewnick, F., Hings, S. S., DeCarlo, P. F., Jayne, J. T., Gonin, M., Fuhrer, K., Weimer, S.,

17   Jimenez, J. L., Demerjian, K. L., Borrmann, S., and Worsnop, D. R.: A new time-of-flight

18   aerosol mass spectrometer (ToF-AMS) – instrument description and first field deployment,

19   Aerosol Sci. Tech., 39, 637–658, 2005.

20   Drobinski, P., Said, F., Arteta, J., Augustin, P., Bastin, S., Brut, A., Caccia, J. L., Campistron,

21   B., Cautenet, S., Colette, A., Coll, I., Corsmeier, U., Cros, B., Dabas, A., Delbarre, H.,

22   Dufour, A., Durand, P., Guenard, V., Hasel, M., Kalthoff, N., Kottmeier, C., Lasry, F.,

23   Lemonsu, A., Lohou, F., Masson, V., Menut, L., Moppert, C., Peuch, V. H., Puygrenier, V.,

24   Reitebuch, O., and Vautard, R.: Regional transport and dilution during high-pollution

25   episodes in southern France: Summary of findings from the Field Experiment to Constraint

26   Models of Atmospheric Pollution and Emissions Transport (ESCOMPTE), J. Geophys. Res.-

27   Atmos., 112, D13105, doi:10.1029/2006JD007494, 2007.

28   Dzepina, K., Arey, J., Marr, L.C., Worsnop, D.R., Salcedo, D., Zhang, Q., Onasch, T.B.,

29   Molina L.T., Molina M. J., Jimenez, J.L.: Detection of particle-phase polycyclic aromatic

30   hydrocarbons in Mexico City using an aerosol mass spectrometer, International Journal of

31   Mass Spectrometry, 263, 152–170, 2007.

1 El Haddad, I., D'Anna, B., Temime-Roussel, B., Nicolas, M., Boreave, A., Favez, O., Voisin,
2 D., Sciare, J., George, C., Jaffrezo, J.-L., Wortham, H., and Marchand, N.: Towards a better
3 understanding of the origins, chemical composition and aging of oxygenated organic aerosols:
4 case study of a Mediterranean industrialized environment, Marseille, Atmos. Chem. Phys., 13,
5 7875–7894, 2013.

6 El Haddad, I., Marchand, N., Dron, J., Temime-Roussel, B., Quivet, E., Wortham, H.,
7 Jaffrezo, J. L., Baduel, C., Voisin, D., Besombes, J. L., and Gille, G.: Comprehensive primary
8 particulate organic characterization of vehicular exhaust emissions in France, Atmos.
9 Environ., 43, 6190–6198, 2009.

10 El Haddad, I., Marchand, N., Wortham, H., Piot, C., Besombes, J.-L. , Cozic, J., Chauvel,
11 C., Armengaud, A., Robin D., and Jaffrezo, J.-L.: Primary sources of $PM_{2.5}$ organic aerosol in
12 an industrial Mediterranean city, Marseille, Atmos. Chem. Phys., 11, 2039-2058, 2011.

13 Elser, M., Huang, R.-J., Wolf, R., Slowik, J. G., Wang, Q., Canonaco, F., Li, G., Bozzetti, C.,
14 Daellenbach, K. R., Huang, Y., Zhang, R., Li, Z., Cao, J., Baltensperger, U., El-Haddad, I.,
15 and Prévôt, A. S. H.: New insights into PM2.5 chemical composition and sources in two
16 major cities in China during extreme haze events using aerosol mass spectrometry, Atmos.
17 Chem. Phys., 16, 3207-3225, doi:10.5194/acp-16-3207-2016, 2016.

18 Favez, O., El Haddad, I., Piot, C., Boréave, A., Abidi, E., Marchand, N., Jaffrezo, J.-L.,
19 Besombes, J.-L., Personnaz, M.-B., Sciare, J., Wortham, H., George, C., and D'Anna, B.:
20 Inter-comparison of source apportionment models for the estimation of wood burning
21 aerosols during wintertime in an Alpine city (Grenoble, France), Atmos. Chem. Phys., 10,
22 5295–5314, doi:10.5194/acp-10-5295- 2010, 2010.

23 Flaounas, E., Coll, I., Armengaud, A., and Schmechtig, C.: The representation of dust
24 transport and missing urban sources as major issues for the simulation of PM episodes in a
25 Mediterranean area, Atmos. Chem. Phys., 9, 8091–8101, doi:10.5194/acp-9-80912009, 2009.

26 Fountoukis, C., Megaritis, A. G., Skyllakou, K., Charalampidis, P. E., Pilinis, C., Denier van
27 der Gon, H. A. C., Crippa, M., Canonaco, F., Mohr, C., Prévôt, A. S. H., Allan, J. D., Poulain,
28 L., Petäjä, T., Tiitta, P., Carbone, S., Kiendler-Scharr, A., Nemitz, E., O'Dowd, C., Swietlicki,
29 E., and Pandis, S. N.: Organic aerosol concentration and composition over Europe: insights
30 from comparison of regional model predictions with aerosol mass spectrometer factor
31 analysis, Atmos. Chem. Phys., 14, 9061-9076, doi:10.5194/acp-14-9061-2014, 2014.

Garcia, E.: A Tutorial on Correlation Coefficients, http://web.simmons.edu/~benoit/lis642/a-tutorial-on-correlation-coefficients.pdf, pp. 7-8, 2011.

He, L.-Y., Lin, Y., Huang, X.-F., Guo, S., Xue, L., Su, Q., Hu, M., Luan, S.-J., and Zhang, Y.-H.: Characterization of high-resolution aerosol mass spectra of primary organic aerosol emissions from Chinese cooking and biomass burning, Atmos. Chem. Phys., 10, 11535-11543, doi:10.5194/acp-10-11535-2010, 2010.

Hennigan, C. J., Sullivan, A. P., Collett, J. L., and Robinson, A. L.: Levoglucosan stability in biomass burning particles exposed to hydroxyl radicals, Geophys. Res. Lett., 37, L09806, doi:10.1029/2010GL043088, 2010.

Herich, H., Gianini, M. F. D., Piot, C., Mocnik, G., Jaffrezo, J. L., Besombes, J. L., Prévôt, A. S. H., and Hueglin, C.: Overview of the impact of wood burning emissions on carbonaceous aerosols and PM in large parts of the Alpine region, Atmos. Environ., 89, 64–75, doi:10.1016/j.atmosenv.2014.02.008, 2014.

Hildebrandt, L., Kostenidou, E., Lanz, V. A., Prevot, A. S. H., Baltensperger, U., Mihalopoulos, N., Laaksonen, A., Donahue, N. M., and Pandis, S. N.: Sources and atmospheric processing of organic aerosol in the Mediterranean: insights from aerosol mass spectrometer factor analysis, Atmos. Chem. Phys., 11, 12499-12515, doi:10.5194/acp-11-12499-2011, 2011.

Hildebrandt, L., Kostenidou, E., Mihalopoulos, N., Worsnop, D. R., Donahue, N. M., and Pandis, S. N.: Formation of highly oxygen-ated organic aerosol in the atmosphere: Insights from the Finokalia Aerosol Measurement Experiments, Geophys. Res. Lett., 37, L23801, doi:10.1029/2010GL 045193, 2010.

Huang, R.-J., Zhang, Y., Bozzetti, C., Ho, K.-F., Cao, J., Han, Y., Daellenbach, K. R., Slowik, J. G., Platt, S. M., Canonaco, F., Zotter, P., Wolf, R., Pieber, S. M., Bruns, E. A., Crippa, M., Ciarelli, G., Piazzalunga, A., Schwikowski, M., Abbaszade, G., Schnelle-Kreis, J., Zimmermann, R., An, Z., Szidat, S., Baltensperger, U., Haddad, I. E., and Prévôt, A. S. H.: High secondary aerosol contribution to particulate pollution during haze events in China, Nature, 514, 218-222, 2014.

Hildemann, L., M., Rogge, W. F., Cass, G. R., Mazurek, M. A., and Simoneit, B. R. T.: Contribution of primary aerosol emissions from vegetation-derived sources to fine particle

concentrations in Los Angeles. J. Geophys. Res., 101, 19,541-19,549, doi: 10.1029/95JD02136, 2016.

Hoffmann, D., Tilgner A., Iinuma, Y., and Herrmann, H.: Atmospheric stability of levoglucosan: a detailed laboratory and modeling study, Environ. Sci. Technol., 44, 694–699, 2010.

Iinuma, Y., Böge, O., Gräfe, R., and Herrmann, H.: Methyl-nitrocatechols: Atmospheric tracer compounds or biomass burning secondary organic aerosols, Environ. Sci. Technol., 44, 8453–8459, 2010.

Jaffrezo, J. L., Calas, T., and Bouchet, M.: Carboxylic acids measurements with ionic chromatography, Atmos. Environ., 32, 2705–2708, 1998.

Jayne, J. T., Leard, D. C., Zhang, X. F., Davidovits, P., Smith, K. A., Kolb, C. E., and Worsnop, D. R. (2000). Development of an aerosol mass spectrometer for size and composition analysis of submicron particles, Aerosol Sci. Technol. 33, 49–70, 2000.

Jimenez, J. L., Canagaratna, M. R., Donahue, N. M., Prevot, A. S. H., Zhang, Q., Kroll, J. H., DeCarlo, P. F., Allan, J. D., Coe, H., Ng, N. L., Aiken, A. C., Docherty, K. S., Ulbrich, I. M., Grieshop, A. P., Robinson, A. L., Duplissy, J., Smith, J. D., Wilson, K. R., Lanz, V. A., Hueglin, C., Sun, Y. L., Tian, J., Laaksonen, A., Raatikainen, T., Rautiainen, J., Vaattovaara, P., Ehn, M., Kulmala, M., Tomlinson, J. M., Collins, D. R., Cubison, M. J., Dunlea, E. J., Huffman, J. A., Onasch, T. B., Alfarra, M. R., Williams, P. I., Bower, K., Kondo, Y., Schneider, J., Drewnick, F., Borrmann, S., Weimer, S., Demerjian, K., Salcedo, D., Cottrell, L., Griffin, R., Takami, A., Miyoshi, T., Hatakeyama, S., Shimono, A., Sun, J. Y., Zhang, Y. M., Dzepina, K., Kimmel, J. R., Sueper, D., Jayne, J. T., Herndon, S. C., Trimborn, A. M., Williams, L. R., Wood, E. C., Middlebrook, A. M., Kolb, C. E., Baltensperger, U., and Worsnop, D. R.: Evolution of organic aerosols in the atmosphere, Science, 326, 1525–1529, 2009.

Karanasiou, A., Diapouli, E., Cavalli, F., Eleftheriadis, K., Viana, M., Alastuey, A., Querol1, X., and Reche, C.: On the quantification of atmospheric carbonate carbon by thermal/optical analysis protocols, Atmos. Meas. Tech., 4, 2409–2419, 2011

Laden, F., Neas, L. M., Dockery, D. W., and Schwartz, J.: Association of fine particulate matter from different sources with daily mortality in six US cities, Environ. Health Perspect. 108:941-947, 2000.

Lanz, V. A., Alfarra, M. R., Baltensperger, U., Buchmann, B., Hueglin, C., and Prevot, A. S. H.. Source apportionment of submicron organic aerosols at an urban site by factor analytical modelling of aerosol mass spectra, Atmos. Chem. Phys. 7:1503-1522, 2007.

Lanz, V. A., M. R. Alfarra, U. Baltensperger, B. Buchmann, C. Hueglin, S. Szidat, M. N. Wehrli, L. Wacker, S. Weimer, A. Caseiro, H. Puxbaum, and A. S. H. Prevot: Source attribution of submicron organic aerosols during wintertime inversions by advanced factor analysis of aerosol mass spectra, Envir. Sci. Tech., 42, 214-220, 2008.

Lee, A. K. Y., Herckes, P., Leaitch, W. R., Macdonald, A. M., and Abbatt, J. P. D.: Aqueous OH oxidation of ambient organic aerosol and cloud water organics: Formation of highly oxidized products, Geoph. Res. Lett., 38, L11 805, doi: 10.1029/2011GL047439, 2011.

Li, W., Peng, Y., and Bai, Z.: Distributions and sources of n-alkanes in $PM_{2.5}$ at urban, industrial and coastal sites in Tianjin, China, J. Environ. Sci., 22, 1551-1557, 2010.

Lohmann, U., Broekhuizen, K., Leaitch, R., Shantz, N., and Abbatt, J.: How efficient is cloud droplet formation of organic aerosols?, Geophys. Res. Lett. 31, L05108, doi: 10.1029/2003GL018999, 2004.

Middlebrook, A.M., Bahrein, R., Jimenez, J.L., and Canagaratna, M.R.: Evaluation of composition-dependent collection efficiencies for the Aerodyne aerosol mass spectrometer using field data, Aerosol Sci. and Tech., 46, 258-271, 2012.

Mihara, T. and Mochida, M.: Characterization of solvent-extractable organics in urban aerosols based on mass spectrum analysis and hygroscopic growth measurement, Environ. Sci. Technol., 45, 9168–9174, 2011.

Minguillón M. C., Pérez N., Marchand N., Bertrand A., Temime-Roussel B., Agrios K., Szidat S., van Drooge B., Sylvestre S., Alastuey A., Reche C., Ripoll A., Marco E., Grimalt J. O., and Querol X.. Secondary organic aerosol origin in an urban environment: influence of biogenic and fuel combustion precursors. Faraday Discussions, 189, 337-359, 2016.

Minguillón, M. C., Perron, N., Querol, X., Szidat, S., Fahrni, S. M., Alastuey, A., Jimenez, J. L., Mohr, C., Ortega, A. M., Day, D. A., Lanz, V. A., Wacker, L., Reche, C., Cusack, M., Amato, F., Kiss, G., Hoffer, A., Decesari, S., Moretti, F., Hillamo, R., Teinila, K., Seco, R., Penuelas, J., Metzger, A., Schallhart, S., Muller, M., Hansel, A., Burkhart, J. F., Baltensperger, U., and Prevot, A. S. H.: Fossil versus contemporary sources of fine elemental

and organic carbonaceous particulate matter during the DAURE campaign in Northeast Spain, Atmos. Chem. Phys., 11, 12067-12084, 2011.

Minguillón, M. C., Ripoll, A., Pérez, N., Prévôt, A. S. H., Canonaco, F., Querol, X., and Alastuey, A.: Chemical characterization of submicron regional background aerosols in the western Mediterranean using an Aerosol Chemical Speciation Monitor, Atmos. Chem. Phys., 15, 6379-6391, 2015.

Mohr, C., DeCarlo, P. F., Heringa, M. F., Chirico, R., Slowik, J. G., Richter, R., Reche, C., Alastuey, A., Querol, X., Seco, R., Penuelas, J., Jimenez, J. L., Crippa, M., Zimmermann, R., Baltensperger, U., and Prevot, A. S. H.: Identification and quantification of organic aerosol from cooking and other sources in Barcelona using aerosol mass spectrometer data, Atmos. Chem. Phys., 12, 1649-1665, 2012.

Mohr, C., Huffman, J. A., Cubison, M. J., Aiken, A. C., Docherty, K. S., Kimmel, J. R., Ulbrich, I. M., Hannigan, M., and Jimenez, J. L.: Characterization of primary organic aerosol emissions from meat cooking, trash burning, and motor vehicles with high resolution aerosol mass spectrometry and comparison with ambient and chamber observations, Environ. Sci. Technol., 43, 2443–2449, 2009.

Paatero, P.: Least squares formulation of robust non-negative factor analysis, Chemom. Intell. Lab. Syst., 37, 23–35, 1997.

Paatero, P.: The multilinear engine - A table-driven, least squares program for solving multilinear problems, including the n-way parallel factor analysis model, J. Comput. Graph. Stat., 8, 854-888, 1999.

Paatero, P. and Tapper, U.: Positive matrix factorization - a nonnegative factor model with optimal utilization of error-estimates of data values, Environmetrics, 5, 111-126, 1994.

Park, S.-S., Cho, S. Y., Jo, M. R., Gong, B. J., Park, J. S., and Lee, S. J.: Field evaluation of a near–real time elemental monitor and identification of element sources observed at an air monitoring supersite in Korea, Atmos Pollut Res., 5, 119-128, doi:10.5094/APR.2014.015, 2014.

Pieber, S. M., El Haddad, I., Slowik, J. G., Canagaratna, M. R., Jayne, J. T., Platt, S. M., Bozzetti, C., Daellenbach, K. R., Fröhlich, R., Vlachou, A., Klein, F., Dommen, J., Miljevic, B., Jimenez, J. L., Worsnop, D. R., Baltensperger, U., and Prévôt, A. S. H.: Inorganic salt

1   interference on CO_2^+ in Aerodyne AMS and ACSM organic aerosol composition studies,

2   Environ. Sci. Technol., 50, 10494-10503, DOI: 10.1021/acs.est.6b01035, 2016.

3   Piot, C., Jaffrezo, J.-L., Cozic, J., Pissot, N., El Haddad, I., Marchand, N., and Besombes, J.-

4   L.: Quantification of levoglucosan and its isomers by High Performance Liquid

5   Chromatography – Electrospray Ionization tandem Mass Spectrometry and its applications to

6   atmospheric and soil samples, Atmos. Meas. Tech., 5, 141–148, doi:10.5194/amt-5-141-2012,

7   2012.

8   Poulain, L., Iinuma, Y., Müller, K., Birmili, W., Weinhold, K., Brüggemann, E., Gnauk, T.,

9   Hausmann, A., Löschau, G., Wiedensohler, A., and Herrmann, H.: Diurnal variations of

10   ambient particulate wood burning emissions and their contribution to the concentration of

11   polycyclic aromatic hydrocarbons (PAHs) in Seiffen, Germany, Atmos. Chem. Phys., 11,

12   12697-12713, doi:10.5194/acp-11-12697-2011, 2011.

13   Rocke, D. M., and Lorenzato, S.: A two-component model for measurement error in

14   analytical chemistry, Technometrics, 37, 176-184, 1995.

15   Salameh, D., Detournay, A., Pey, J., Pérez, N., Liguori, F., Saraga, D., Bove, M. C., Brotto,

16   P., Cassola, F., Massabò, D., Latella, A., Pillon, S., Formenton, G., Patti, S., Armengaud, A.,

17   Piga, D., Jaffrezo, J.-L., Bartzis, J., Tolis, E., Prati, P., Querol, X., Wortham, H., Marchand,

18   N.: $PM_{2.5}$ chemical composition in five European Mediterranean cities: a 1-year study,

19   Atmos. Res., 155, 102-117, 2015.

20   Salameh, D., Pey, J., Bozzetti, C., El Haddad, I., Detournay, A., Sylvestre, A., Canonaco, F.,

21   Armengaud, A., Piga, D., Robin, D., Prévôt, A. S. H., Jaffrezo, J.-L., Wortham, H., and

22   Marchand, N.: Sources of $PM_{2.5}$ at an urban-industrial Mediterranean city: an application of

23   ME-2 model to $PM_{2.5}$ offline dataset from Marseille (France), *in prep.*

24   Schauer, J. J., Kleeman, M. J., Cass, G. R., Simoneit, B. R. T.: Measurement of emissions

25   from air pollution sources. 3. C1-C29 organic compounds from fireplace combustion of

26   wood, Environ. Sci. Technol., 35, 1716–1728, 2001.

27   Schwarze, P. E., Ovrevik, J., Lag, M., Refsnes, M., Nafstad, P., Hetland, R. B., Dybing, E.

28   (2006). Particulate matter properties and health effects: consistency of epidemiological and

29   toxicological studies, Hum. Exp. Toxicol., 25, 559-579, 2006.

30   Seinfeld, J. H. and Pandis, S. N: Atmospheric chemistry and physics: from air pollution to

31   climate change, John Wiley, second Edn., New York, 2006.

Setyan, A., Zhang, Q., Merkel, M., Knighton, W. B., Sun, Y., Song, C., Shilling, J. E., Onasch, T. B., Herndon, S. C., Worsnop, D. R., Fast, J. D., Zaveri, R. A., Berg, L. K., Wiedensohler, A., Flowers, B. A., Dubey, M. K., and Subramanian R.: Characterization of submicron particles influenced by mixed biogenic and anthropogenic emissions using high-resolution aerosol mass spectrometry: results from CARES, Atmos. Chem. Phys., 12, 8131-8156, 2012.

Simoneit, B. R. T., Schauer, J. J., Nolte, C. G., Oros, D. R., Elias, V. O., Fraser, M. P., Rogge, W. F., and Cass, G. R.: Levoglucosan, a tracer for cellulose in biomass burning and atmospheric particles, Atmos. Environ., 33, 173-182, 1998.

Simoneit, B. R. T., Sheng, G., Chen, X., Fu, J., Zhang, J. and Xu, Y.: Molecular marker study of extractable organic matter in aerosols from urban areas of China, Atmos. Environ. Part A. Gen. Top., 25(10), 2111–2129, doi:10.1016/0960-1686(91)90088-O, 1991.

Slowik, J. G., Vlasenko, A., McGuire, M., Evans, G. J., and Abbatt, J. P. D.: Simultaneous factor analysis of organic particle and gas mass spectra: AMS and PTR-MS measurements at an urban site, Atmos. Chem. Phys, 10:1969-1988, 2010.

Sullivan, A. P., Holden, A. S., Patterson, L. A., McMeeking, G. R., Kreidenweis, S. M., Malm, W. C., Hao, W. M., Wold, C. E., and Collett Jr., J. L.: A method for smoke marker measurements and its potential application for determining the contribution of biomass burning from wildfires and prescribed fires to ambient PM2.5 organic carbon, J. Geophys. Res., 113, D22302, doi:10.1029/2008JD010216, 2008.

Sun, Y., Zhang, Q., Zheng, M., Ding, X., Edgerton, E. S., and Wang, X.: Characterization and source apportionment of water-soluble organic matter in atmospheric fine particles (PM2.5) with high-resolution aerosol mass spectrometry and GC-MS, Environ. Sci. Technol., 45, 4854–4861, 2011.

Ulbrich, I. M., Canagaratna, M. R., Zhang, Q., Worsnop, D. R., and Jimenez, J. L.: Interpretation of organic components from positive matrix factorization of aerosol mass spectrometric data, Atmos. Chem. Phys., 9, 2891-2918, 2009.

Ulevicius, V., Byčenkienė, S., Bozzetti, C., Vlachou, A., Plauškaitė, K., Mordas, G., Dudoitis, V., Abbaszade, G., Remeikis, V., Garbaras, A., Masalaite, A., Blees, J., Fröhlich, R., Dällenbach, K. R., Canonaco, F., Slowik, J. G., Dommen, J., Zimmermann, R., Schnelle-Kreis, J., Salazar, G. A., Agrios, K., Szidat, S., El Haddad, I., and Prévôt, A. S. H.: Fossil and

1 non-fossil source contributions to atmospheric carbonaceous aerosols during extreme spring

2 grassland fires in Eastern Europe. Atmos. Chem. Phys., 16, 5513-5529, 2016.

3 Weitkamp, E. A., Lipsky, E. M., Pancras, P. J., Ondov, J. M., Polidori, A., Turpin, B. J., and

4 Robinson, A. L.: Fine particle emission profile for a large coke production facility based on

5 highly time-resolved fence line measurements, Atmos. Environ., 39, 6719–6733, 2005.

6 Zar, J. H., Biostatistical analysis, 4th ed., 929 pp., Prentice Hall, Englewood Cliffs, New

7 Jersey, 1999.

8 Zotter, P., Ciobanu, V. G., Zhang, Y. L., El-Haddad, I., Macchia, M., Daellenbach, K. R.,

9 Salazar, G. A., Huang, R.-J., Wacker, L., Hueglin, C., Piazzalunga, A., Fermo,

10 P.,Schwikowski, M., Baltensperger, U., Szidat, S., and Prévôt, A. S. H.: Radiocarbon analysis

11 of elemental and organic carbon in Switzerland during winter-smog episodes from 2008 to

12 2012 – Part 1: Source apportionment and spatial variability, Atmos. Chem. Phys., 14, 13551–

13 13570, doi:10.5194/acp-14-13551-2014, 2014.
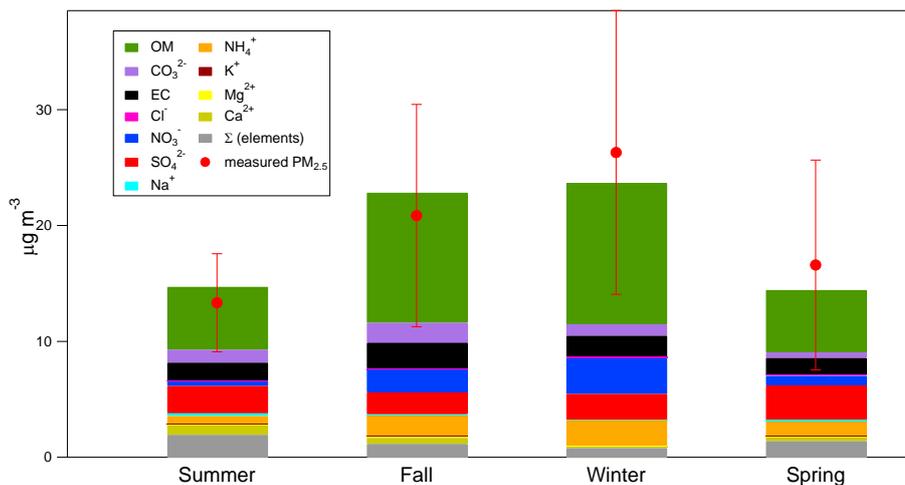
3   Figure 1. PM$_{2.5}$ composition: stacked average seasonal concentrations. Measured PM$_{2.5}$ error

4   bars represent the seasonal standard deviation. OM was estimated as the sum of the offline-

5   AMS source apportionment factors.
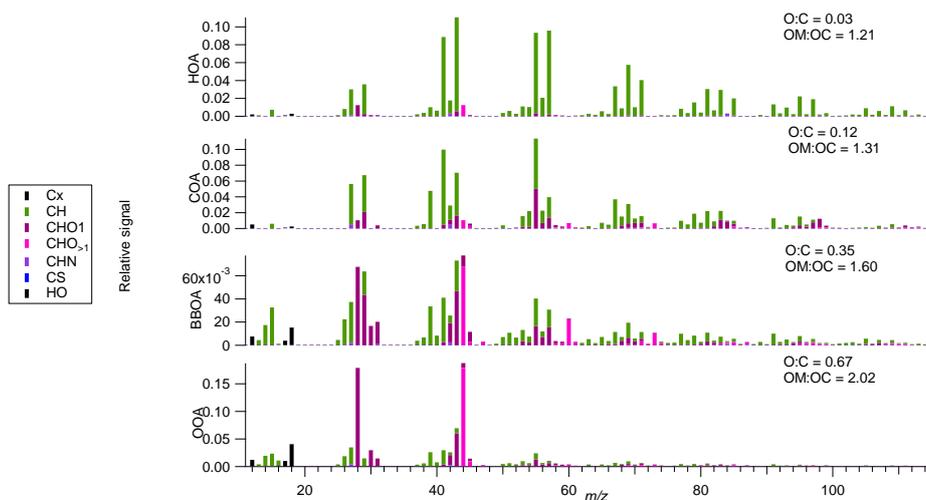
8   Figure 2. Online-AMS: average PMF factor mass spectra.
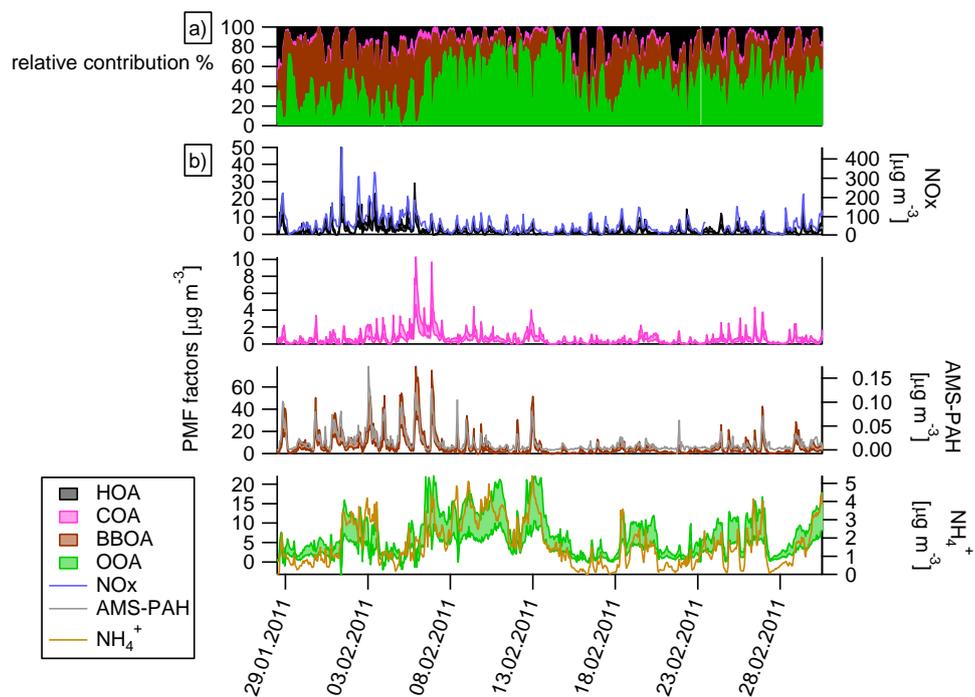
2   Figure 3. Online-AMS: a) PMF factors relative contributions. b) Time series of PMF factors

3   and corresponding tracers. Shaded areas denote the model uncertainties.
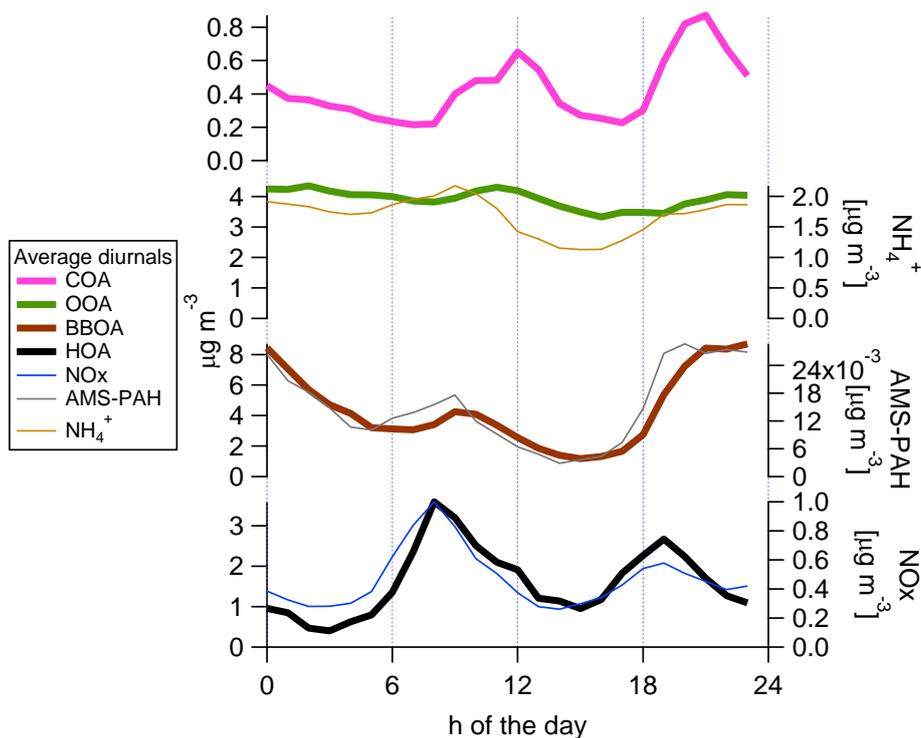
2   Figure 4. Online-AMS: average diurnal cycles of PMF factors and corresponding tracers.
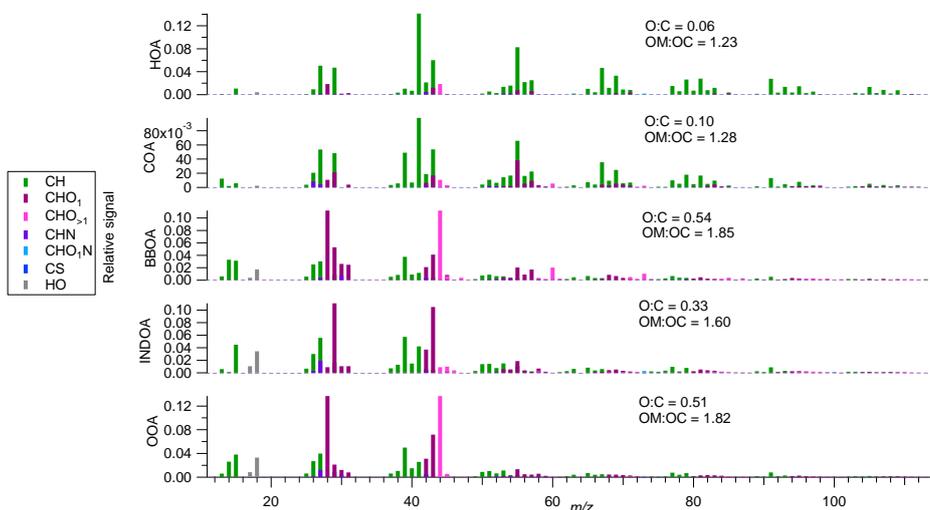
5   Figure 5. Offline-AMS: water soluble average mass spectra.
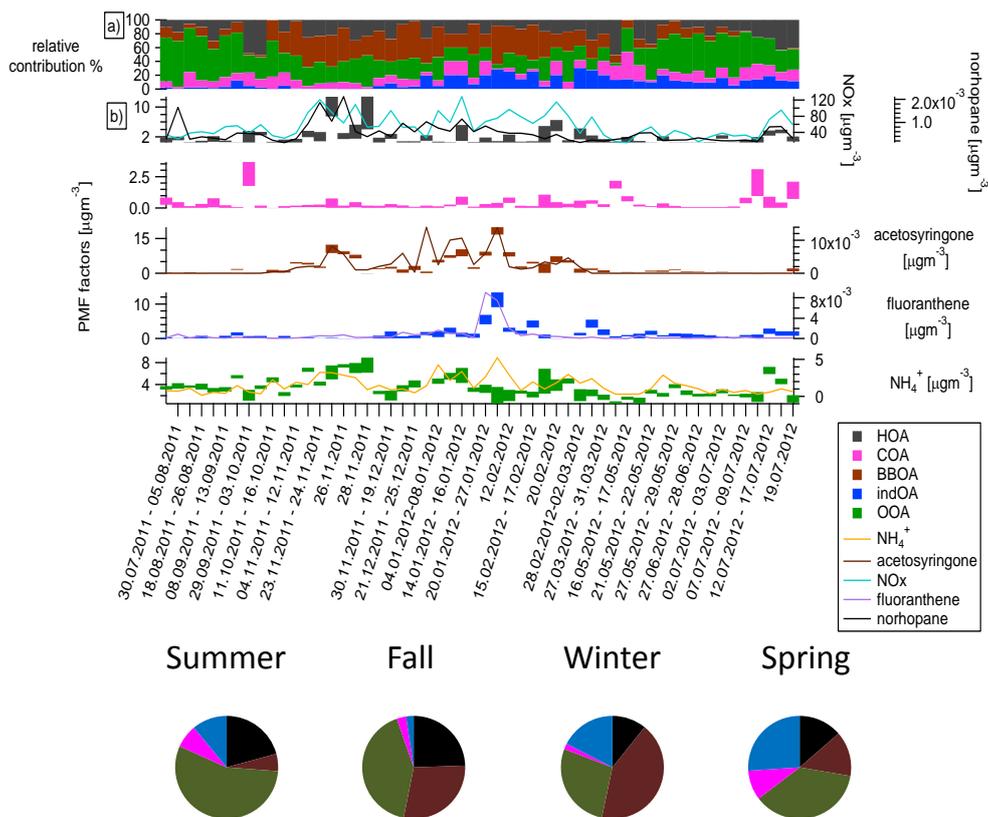
4   Figure 6. Offline-AMS: a) PMF factors relative contributions. b) Time series of PMF factors

5   and corresponding tracers. Bars denote the model uncertainties.
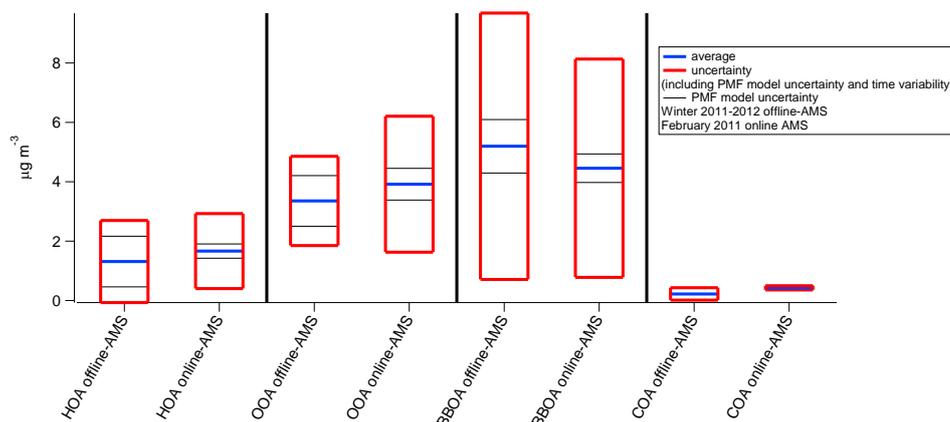
2   Figure 7. Online (PM$_1$) and offline-AMS (PM$_{2.5}$) comparison. Bars represent the error

3   including temporal variability and model uncertainty.
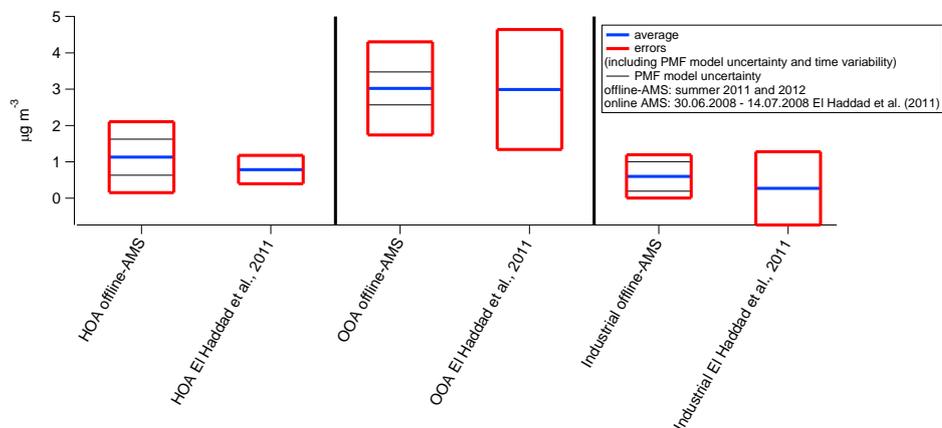
5   Figure 8. Online (PM$_1$, El Haddad et al., 2013) and offline-AMS (PM$_{2.5}$) comparison. For

6   offline-AMS bars represent the error including temporal variability and model uncertainty.

7   For online-AMS bars represents only the temporal variability.
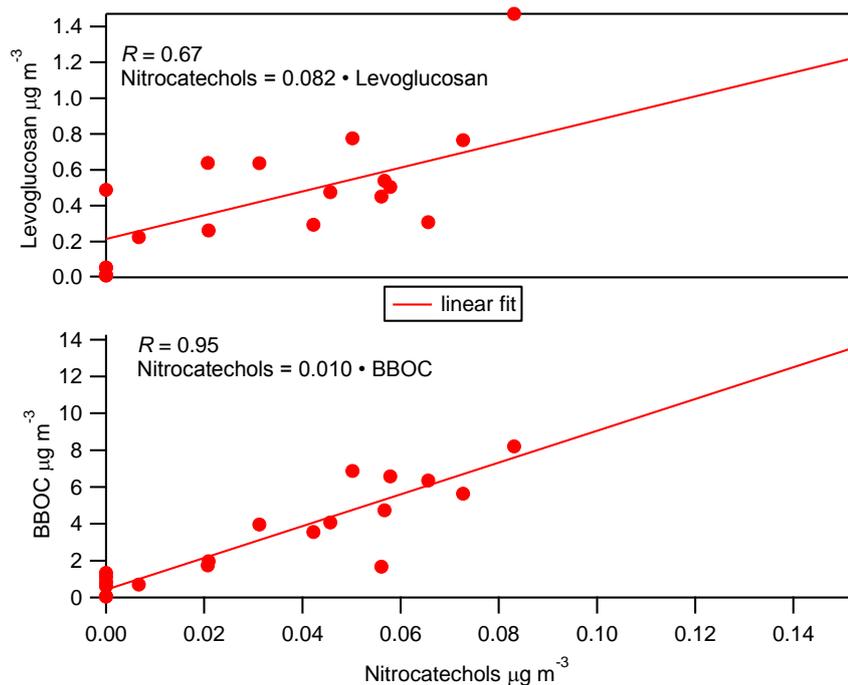
2   Figure 9. Correlation between the sum of nitrocatechols (Table S1) with levoglucosan and

3   BBOC.
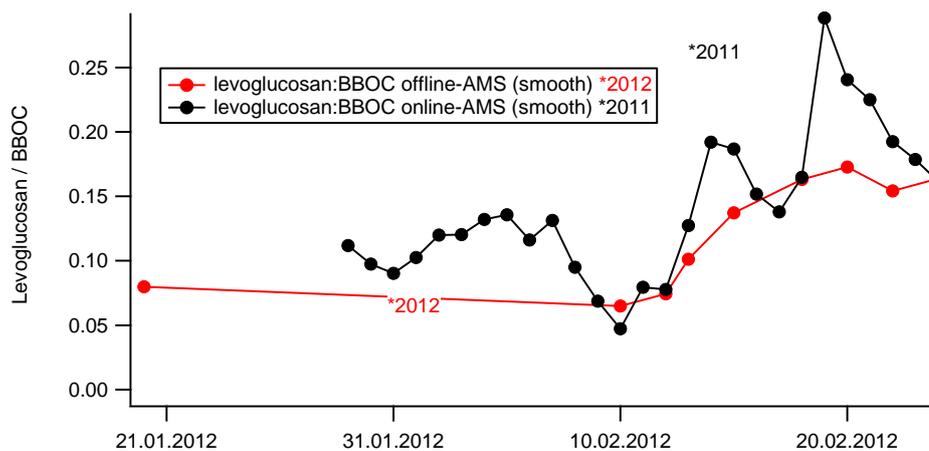
5   Figure 10: Offline-AMS (February 2012) and online-AMS (February 2011) smoothed time-

6   dependent levoglucosan:BBOC ratios. We note that the levoglucosan:BBOC comparison

7   should not be considered on a day-to-day basis where the levoglucosan:BBOC ratio in the two

8   different years can be coincidentially equal or different, but rather on a monthly time scale

1 where, as discussed in the manuscript, we observed a statistically significant (p=0.05)

2 evolution of the levoglucosan:BBOC ratio which is similarly captured by the two models.
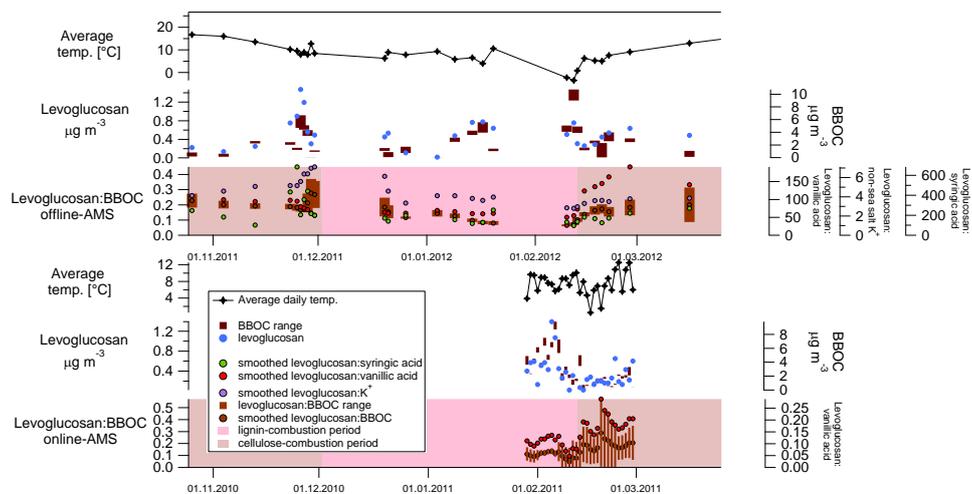
5 Figure 11: Online- and offline-AMS time-dependent levoglucosan:BBOC,

6 levoglucosan:vanillic acid, levoglucosan:syringic acid, and levoglucosan:K$^+$ ratios.